

Simultaneously determine elastic impedance and shape by a Newton-type iterative method

Yao Sun^{†,*}, Pan Wang[†]

*Corresponding author: sunyao10@mails.jlu.edu.cn

[†] College of Science, Civil Aviation University of China, Tianjin, China

Abstract. This paper focuses on an indirect boundary integral equation method for the inverse elastic impedance and the geometry problem by a Cauchy data pair on the access part of the boundary in a two-dimensional case. A uniqueness result is given for the corresponding problem, and a non-iterative algorithm is proposed to solve the data completion problem using a Cauchy data pair on an accessible part of the solution domain's boundary. Next, we introduce a Newton-type iterative method for reconstructing the missing boundary and the impedance function using the completion data on the unknown boundary, which is governed by a specific type of boundary conditions. This method should not deal with the singularities of the kernels of hypersingular integral from Fréchet derivative. Finally, we provide several examples to demonstrate the effectiveness and accuracy of the proposed method.

Key words: Indirect boundary integral equation, Cauchy data, Collocation method.

1 Introduction

The study of elastic waves has become an important research area in mathematical physics. This type of problem is widely used in nondestructive testing, medical imaging and seismic exploration [3,4]. A typical inverse problem involves determining the boundary shape of an elastic obstacle from the Cauchy data on the accessible part boundary. In practical applications such as physics and engineering, due to multiple factors including measurement technology limitations, it is not possible to obtain complete information about the surface of obstacles. Therefore, it is necessary to consider supplementing the information about the non-accessible/missing part boundary. In the case of electrostatics, the model yields an inverse boundary value problem related to the Laplace equation. In the case of elastic obstacles, an inverse boundary value problem arises in relation to the Navier equation. Literature references can be consulted for both cases [1, 13, 23, 35]. The inverse acoustic scattering can be found in [20, 21, 29]. In many inverse problems, it is not realistic

to assume that the boundary conditions are known. This is the physical motivation for simultaneously determine the elastic impedance and shape stems from the practical problems. Carrying this idea further we can ask if it is possible, by modifying the impedance values of the boundary of an obstacle, to make it appear from an experiment standpoint as some object of a different shape.

Various methods have been investigated in recent years to solve the inverse elastic obstacle problem. In [28], Li et al. investigate the inverse elastic scattering problem for bi-periodic surfaces in three dimensions. A local uniqueness is proved for the inverse problem when the scattering surface has been assumed to be a small and smooth perturbation of a rigid planar surface. Louër [32,33] derives the domain derivatives of elastic scattering, which can be employed to reconstruct unknown elastic obstacles through the design of gradient descent methods. Additionally, Alves and Kress [2] examine a linear sampling method, which is based on far-field operator decomposition, for inverse elastic scattering problem. Factorization method has been extensively researched by Hu et al. in [17,18]. The inverse elastic impedance problem, as discussed in [30,42], has found widespread application in seismology, oilfield exploration, and other related fields. There are some other research papers for the inverse elastic problem, such as [14,31,40] and etc.

In [25,27], Kress and Rundell consider the inverse problems of time-harmonic acoustic or electromagnetic waves. A regularized Newton iteration is given to solve the inverse problem of simultaneously determining the impedance and shape of a two-dimensional scatterer, which is based on a knowledge of the far-field pattern. The main idea is to establish the ill-posed nonlinear equation for the operator that maps the boundary and the boundary impedance of the scatterer onto the far-field pattern. Later, Kress and Rundell [26] determine the shape of a perfectly conducting inclusion via a pair of nonlinear and ill-posed integral equations for the unknown boundary. The integral equations can be solved by the linearization corresponding to the regularized Newton iterations. This idea is to extend by Cakoni and Kress [7] to a simply connected planar domain from a pair of Cauchy data on the known boundary curve. This method is also used to complete the Cauchy data on the unknown boundary curve, and then an impedance profile is given by a point to point method. Thus the boundary curve is to recover by a known impedance profile.

Motivated by the idea in [25] proposed by Kress and Rundell, we aim to demonstrate a Newton-type iterative method for reconstructing the elastic impedance function and the shape of the elastic body based on the integral equations. Different from the previous work [25] by a direct integral approach for the mixed problem, we consider an indirect integral equation by the approach of having an integral operator defined on a virtual boundary enclosing the scatterer. Though the direct integral approach would provide some more information about the curve. It should deal with the singularities of the kernels on the boundary especially the strongly singular integral resulting the hypersingular integral from Fréchet derivative. The indirect integral approach will easily give the Fréchet derivative of the boundary integral operator. The contributions of this paper are as follows:

- (i) A uniqueness result is given for the corresponding problem.
- (ii) A Newton-type iterative method for reconstructing the boundary and the impedance function.

The paper is organized as follows. In Section 2, we introduce the inverse impedance problem and the inverse shape problem. In Section 3, some theoretical results including a unique result are given by introducing the Helmholtz decomposition of the displacement. Then in Section 4, we specifically demonstrate linearization of the integral equations and the Newton-type iterative method for solving inverse shape problem. Then some numerical examples are provided to demonstrate the effectiveness of the proposed linearized iterative scheme.

2 Problem formulation

Let $D \subset \mathbb{R}^2$ be an open bounded domain with Lipschitz boundary ∂D , which is occupied by homogeneous and isotropic elastic medium with the density ρ . Assuming that the boundary ∂D be analytical and can be given as $\partial D = \Gamma_0 \cup \Gamma_m$, $\Gamma_0 \cap \Gamma_m = \emptyset$, where Γ_0 and Γ_m are the known part and the unknown part of the boundary ∂D . λ and μ , usually called Lemé constants, satisfy $\mu > 0$ and $\lambda + \mu > 0$. ω designates the frequency of vibration. The displacement field \mathbf{u} corresponding to the stress tensor $\boldsymbol{\sigma}(\mathbf{u})$ inside D satisfies the following Navier equation

$$\nabla \cdot \boldsymbol{\sigma}(\mathbf{u}) + \rho\omega^2\mathbf{u} = 0, \quad \text{in } D. \quad (2.1)$$

For a linear isotropic elastic medium, the components of the stress tensor $\boldsymbol{\sigma}(\mathbf{u})$ be

$$\sigma_{ij} = \lambda\delta_{ij}\varepsilon_{\ell\ell} + 2\mu\varepsilon_{ij}, \quad i, j = 1, 2,$$

with the strain tensor ε_{ij} given by

$$\varepsilon_{ij} = \frac{1}{2} \left(\frac{\partial u_i}{\partial x_j} + \frac{\partial u_j}{\partial x_i} \right),$$

where δ_{ij} is the Kronecker delta function.

On the boundary ∂D , the displacement \mathbf{u} satisfies the following boundary conditions:

- Dirichlet boundary condition on Γ_0

$$\mathbf{u} = \mathbf{f}(\mathbf{x}, \omega), \quad \text{on } \Gamma_0. \quad (2.2)$$

- Impedance boundary condition on Γ_m

$$T_n \mathbf{u} + i\omega\chi\mathbf{u} = \mathbf{g}(\mathbf{x}, \omega), \quad \text{on } \Gamma_m. \quad (2.3)$$

The impedance function $\chi \geq 0$ is continuous.

For a fixed point $\mathbf{x} \in \partial D$, T the traction operator, defined on the boundary ∂D , is given by

$$(T_n \mathbf{u})_\ell := \lambda n_\ell \frac{\partial u_j}{\partial x_j} + \mu n_j \left(\frac{\partial u_\ell}{\partial x_j} + \frac{\partial u_j}{\partial x_\ell} \right), \quad \ell = 1, 2,$$

where \mathbf{n} is the unit outward normal vector.

For a scalar function w , we have

$$\nabla w = \left(\frac{\partial w}{\partial x_1}, \frac{\partial w}{\partial x_2} \right)^\top, \quad \nabla^\perp w = \left(\frac{\partial w}{\partial x_2}, -\frac{\partial w}{\partial x_1} \right)^\top.$$

It is well-known that the displacement field \mathbf{u} can be split into the compressional and shear parts, i.e. the Helmholtz decomposition as follows

$$\mathbf{u} = \nabla u_p + \nabla^\perp u_s. \quad (2.4)$$

u_p and u_s , respectively, are the solutions of the following Helmholtz equations

$$\Delta u_p + \kappa_p^2 u_p = 0, \quad \Delta u_s + \kappa_s^2 u_s = 0.$$

κ_p and κ_s are the wave numbers of the compressional part and the shear part with the values $\kappa_p = \sqrt{\frac{\rho\omega^2}{\lambda+2\mu}}$ and $\kappa_s = \sqrt{\frac{\rho\omega^2}{\mu}}$.

Together with the equations (2.1) – (2.4), we get the problem considered as follows

$$\begin{cases} \Delta u_p + \kappa_p^2 u_p = 0, & \text{in } D, \\ \Delta u_s + \kappa_s^2 u_s = 0, & \text{in } D, \\ \mathbf{u} = \mathbf{f}(\mathbf{x}, \omega), & \text{on } \Gamma_0, \\ T_n \mathbf{u} + i\omega\chi \mathbf{u} = \mathbf{g}(\mathbf{x}, \omega), & \text{on } \Gamma_m. \end{cases} \quad (2.5)$$

Inverse Problem: The inverse problem we considered is to determine the shape of the unknown portion Γ_m and impedance function χ from the displacement field $\mathbf{f}(\mathbf{x}, \omega)$ and the (measured) traction $\mathbf{t}(\mathbf{x}, \omega) = T_n \mathbf{u}$ on Γ_0 .

3 Theoretical results

We denote $\Phi(\kappa|\mathbf{x} - \mathbf{y}|)$ be the fundamental solution of the Helmholtz equation associated with the wavenumber κ , namely

$$\Phi(\kappa|\mathbf{x} - \mathbf{y}|) = \frac{i}{4} H_0^{(1)}(\kappa|\mathbf{x} - \mathbf{y}|), \quad (3.1)$$

with $H_0^{(1)}$ be the Hankel function of the first kind of order zero.

The displacement is $\mathbf{u} = \nabla u_p + \nabla^\perp u_s$. The vector components of the displacement \mathbf{u} will be

$$u_p(\mathbf{x}) = \int_{\partial B} \Phi(\kappa_p |\mathbf{x} - \mathbf{y}|) \varphi_1(\mathbf{y}) ds(\mathbf{y}), \quad \mathbf{x} \in D, \quad (3.2)$$

and

$$u_s(\mathbf{x}) = \int_{\partial B} \Phi(\kappa_s |\mathbf{x} - \mathbf{y}|) \varphi_2(\mathbf{y}) ds(\mathbf{y}), \quad \mathbf{x} \in D, \quad (3.3)$$

where φ_1, φ_2 are the density functions, $D \subset\subset B$, ∂B is the so called virtual boundary.

Combining (3.2), (3.3) and the definition of ∇^\perp for a scalar function, we have

$$\mathbf{u}(\mathbf{x}) = \int_{\partial B} \mathbb{E}(\mathbf{x}, \mathbf{y}) \boldsymbol{\varphi}(\mathbf{y}) ds(\mathbf{y}), \quad \mathbf{x} \in D, \quad (3.4)$$

with $\boldsymbol{\varphi} = (\varphi_1, \varphi_2)^\top$ and

$$\mathbb{E}(\mathbf{x}, \mathbf{y}) = \begin{pmatrix} \frac{\partial \Phi(\kappa_p |\mathbf{x} - \mathbf{y}|)}{\partial x_1} & \frac{\partial \Phi(\kappa_s |\mathbf{x} - \mathbf{y}|)}{\partial x_2} \\ \frac{\partial \Phi(\kappa_p |\mathbf{x} - \mathbf{y}|)}{\partial x_2} & -\frac{\partial \Phi(\kappa_s |\mathbf{x} - \mathbf{y}|)}{\partial x_1} \end{pmatrix}.$$

Denote the unit outward normal vector by \mathbf{n} at $\mathbf{x} \in \partial D$, and the corresponding traction $T_{n_x} \mathbf{u}$ is given

$$(T_{n_x} \mathbf{u})(\mathbf{x}) = \int_{\partial B} \mathbb{T}(\mathbf{x}, \mathbf{y}) \boldsymbol{\varphi}(\mathbf{y}) ds(\mathbf{y}), \quad \mathbf{x} \in \partial D, \quad (3.5)$$

where the elements of the matrix $\mathbb{T}(\mathbf{x}, \mathbf{y})$ are given by

$$\begin{aligned} \mathbb{T}_{1j}(\mathbf{x}, \mathbf{y}) &= \left[(\lambda + 2\mu) \frac{\partial \mathbb{E}_{1j}(\mathbf{x}, \mathbf{y})}{\partial x_1} + \lambda \frac{\partial \mathbb{E}_{2j}(\mathbf{x}, \mathbf{y})}{\partial x_2} \right] n_1 + \mu \left(\frac{\partial \mathbb{E}_{1j}(\mathbf{x}, \mathbf{y})}{\partial x_2} + \frac{\partial \mathbb{E}_{2j}(\mathbf{x}, \mathbf{y})}{\partial x_1} \right) n_2, \\ \mathbb{T}_{2j}(\mathbf{x}, \mathbf{y}) &= \mu \left(\frac{\partial \mathbb{E}_{1j}(\mathbf{x}, \mathbf{y})}{\partial x_2} + \frac{\partial \mathbb{E}_{2j}(\mathbf{x}, \mathbf{y})}{\partial x_1} \right) n_1 + \left[\lambda \frac{\partial \mathbb{E}_{1j}(\mathbf{x}, \mathbf{y})}{\partial x_1} + (\lambda + 2\mu) \frac{\partial \mathbb{E}_{2j}(\mathbf{x}, \mathbf{y})}{\partial x_2} \right] n_2. \end{aligned}$$

Denote by

$$\mathbf{S}\boldsymbol{\varphi}(\mathbf{x}) := \int_{\partial B} \mathbb{E}(\mathbf{x}, \mathbf{y}) \boldsymbol{\varphi}(\mathbf{y}) ds(\mathbf{y}), \quad \mathbf{x} \in \mathbb{R}^2 \setminus \partial B, \quad (3.6)$$

$$\mathbb{K}\boldsymbol{\varphi}(\mathbf{x}) := T_{n_x} \int_{\partial B} \mathbb{E}(\mathbf{x}, \mathbf{y}) \boldsymbol{\varphi}(\mathbf{y}) ds(\mathbf{y}), \quad \mathbf{x} \in \partial D \quad (3.7)$$

and

$$\mathbb{S}\boldsymbol{\varphi}(\mathbf{x}) := \int_{\partial B} \mathbb{E}(\mathbf{x}, \mathbf{y}) \boldsymbol{\varphi}(\mathbf{y}) ds(\mathbf{y}), \quad \mathbf{x} \in \partial D. \quad (3.8)$$

We have the following result, and the proof is similar to the proof of three dimensional case [41].

Theorem 1. *The operator \mathcal{S} is compact, injective and has dense range if $\rho\omega^2$ is not a Dirichlet eigenvalue of the negative lamé operator in the interior D .*

On Γ_0 , define the operator \mathcal{N} by

$$\mathcal{N}\boldsymbol{\varphi}(\mathbf{x}) : = \begin{pmatrix} \mathbf{S}\boldsymbol{\varphi}(\mathbf{x}) \\ T_{n_{\mathbf{x}}}\mathbf{S}\boldsymbol{\varphi}(\mathbf{x}) \end{pmatrix}, \quad \mathbf{x} \in \Gamma_0.$$

Theorem 2. *The operator $\mathcal{N} : \mathbf{L}^2(\partial B) \rightarrow \mathbf{H}^{1/2}(\Gamma_0) \times \mathbf{H}^{-1/2}(\Gamma_0)$ is compact, injective and has dense range.*

Proof. The operator $\mathcal{N} : \mathbf{L}^2(\partial B) \rightarrow \mathbf{H}^{1/2}(\Gamma_0) \times \mathbf{H}^{-1/2}(\Gamma_0)$ is compact by the kernel function of \mathcal{N} being analytic [6, Theorem 2.7].

If we let $\mathcal{N}\boldsymbol{\varphi} = 0$, it should be injective by $\boldsymbol{\varphi} = 0$. The uniqueness of the Cauchy problem yields that $\mathbf{S}\boldsymbol{\varphi} = 0$ in D . A unique continuation argument yields that $\mathbf{S}\boldsymbol{\varphi} = 0$ in B .

In fact

$$\mathbf{S}\boldsymbol{\varphi}(\mathbf{x}) = \nabla_{\mathbf{x}} \int_{\partial B} \Phi(\kappa_p|\mathbf{x} - \mathbf{y}|)\varphi_1(\mathbf{y})ds(\mathbf{y}) + \nabla_{\mathbf{x}}^{\perp} \int_{\partial B} \Phi(\kappa_s|\mathbf{x} - \mathbf{y}|)\varphi_2(\mathbf{y})ds(\mathbf{y}). \quad (3.9)$$

Denote

$$\phi(\mathbf{x}) = \int_{\partial B} \Phi(\kappa_p|\mathbf{x} - \mathbf{y}|)\varphi_1(\mathbf{y})ds(\mathbf{y}), \quad \mathbf{x} \in \mathbb{R}^2 \setminus \partial B,$$

and

$$\psi(\mathbf{x}) = \int_{\partial B} \Phi(\kappa_s|\mathbf{x} - \mathbf{y}|)\varphi_2(\mathbf{y})ds(\mathbf{y}), \quad \mathbf{x} \in \mathbb{R}^2 \setminus \partial B,$$

we have

$$\nabla\phi = -\nabla^{\perp}\psi, \quad \text{in } B. \quad (3.10)$$

Taking the dot product with ∇ and ∇^{\perp} , respectively, thus we have

$$\Delta\phi = 0, \quad \Delta\psi = 0, \quad \text{in } B. \quad (3.11)$$

Noting that ϕ and ψ satisfy the Helmholtz equations, we get

$$\phi = \psi = 0, \quad \text{in } B, \quad (3.12)$$

and thus

$$\frac{\partial\phi_-}{\partial\nu} = \frac{\partial\psi_-}{\partial\nu} = 0, \quad \text{on } \partial B, \quad (3.13)$$

where ν denotes the unit outward normal vector defined on ∂B and $-$ denotes the limits as $\mathbf{x} \rightarrow \partial B$ from inside of ∂B .

From the jump relation of the single-layer potential functions (see e.g. [6]), we can get

$$\phi_+ = \phi_- \quad \text{and} \quad \frac{\partial \phi_-}{\partial \nu} - \frac{\partial \phi_+}{\partial \nu} = \varphi_1, \quad \text{on } \partial B, \quad (3.14)$$

where $+$ denotes the limits as $\mathbf{x} \rightarrow \partial B$ from outside of ∂B .

From equation (3.14), we know $\phi_+ = 0$ and $-\frac{\partial \phi_+}{\partial \nu} = \varphi_1$ on ∂B . This means that ϕ satisfies the homogeneous exterior Dirichlet boundary value problem with the Sommerfeld radiation condition, the uniqueness for the exterior Dirichlet problem yields $\phi = 0$ outside of ∂B , and thus $\frac{\partial \phi_+}{\partial \nu} = 0$. Combining with equation (3.14), we have $\varphi_1 = 0$. The same argument will give $\varphi_2 = 0$. Therefore the operator \mathcal{N} is injective.

Next we prove that \mathcal{N} has dense range. We consider the adjoint operator $\mathcal{N}^* : \mathbf{H}^{1/2}(\Gamma_0) \times \mathbf{H}^{-1/2}(\Gamma_0) \rightarrow \mathbf{L}^2(\partial B)$ defined by

$$\langle \mathcal{N}\varphi, [\boldsymbol{\xi}_1, \boldsymbol{\xi}_2] \rangle = \langle \varphi, \mathcal{N}^*[\boldsymbol{\xi}_1, \boldsymbol{\xi}_2] \rangle. \quad (3.15)$$

We want to show that \mathcal{N}^* is injective which implies that \mathcal{N} has dense range.

Let $\mathcal{N}^*(\boldsymbol{\xi}_1, \boldsymbol{\xi}_2) = 0$. Noted that

$$\mathcal{N}^*(\boldsymbol{\xi}_1, \boldsymbol{\xi}_2) = \int_{\Gamma_0} \mathbb{E}^\top(\mathbf{x}, \mathbf{y}) \overline{\boldsymbol{\xi}_1}(\mathbf{x}) ds(\mathbf{x}) + \int_{\Gamma_0} \mathbb{T}^\top(\mathbf{x}, \mathbf{y}) \overline{\boldsymbol{\xi}_2}(\mathbf{x}) ds(\mathbf{x}), \quad \mathbf{y} \in \partial B. \quad (3.16)$$

Denote

$$\mathbf{w}'(\mathbf{y}) = \int_{\Gamma_0} \mathbb{E}^\top(\mathbf{x}, \mathbf{y}) \overline{\boldsymbol{\xi}_1}(\mathbf{x}) ds(\mathbf{x}), \quad \mathbf{y} \in \mathbb{R}^2 \setminus \Gamma_0, \quad (3.17)$$

and

$$\mathbf{w}''(\mathbf{y}) = \int_{\Gamma_0} \mathbb{T}^\top(\mathbf{x}, \mathbf{y}) \overline{\boldsymbol{\xi}_2}(\mathbf{x}) ds(\mathbf{x}), \quad \mathbf{y} \in \mathbb{R}^2 \setminus \Gamma_0. \quad (3.18)$$

We set $\mathbf{W}(\mathbf{y}) = \mathbf{w}'(\mathbf{y}) + \mathbf{w}''(\mathbf{y})$. The components of $\mathbf{W}(\mathbf{y})$ are $W_1(\mathbf{y})$ and $W_2(\mathbf{y})$. $W_1(\mathbf{x})$ satisfies

$$\begin{cases} \Delta W_1 + \kappa_p^2 W_1 = 0, & \text{in } \mathbb{R}^2 \setminus \overline{B}, \\ W_1(\mathbf{y}) = 0, & \text{on } \partial B. \end{cases} \quad (3.19)$$

and the Sommerfeld radiation condition. The uniqueness for the exterior Dirichlet problem yields $W_1(\mathbf{y}) = 0$ outside of ∂B . A unique continuation argument yields that $W_1(\mathbf{y}) = 0$ in $\mathbb{R}^2 \setminus \Gamma_0$, thus also $W_2(\mathbf{y}) = 0$ in $\mathbb{R}^2 \setminus \Gamma_0$.

Denote

$$\widetilde{\mathbf{W}}(\mathbf{y}) = \nabla W_1(\mathbf{y}) + \nabla^\perp W_2(\mathbf{y}), \quad \mathbf{y} \in \mathbb{R}^2 \setminus \Gamma_0, \quad (3.20)$$

we have

$$\widetilde{\mathbf{W}}(\mathbf{y})_+ = \widetilde{\mathbf{W}}(\mathbf{y})_- = 0 \quad \text{and} \quad T_n \widetilde{\mathbf{W}}(\mathbf{y})_+ = T_n \widetilde{\mathbf{W}}(\mathbf{y})_- = 0, \quad \text{on } \Gamma_0. \quad (3.21)$$

On the other hand, we have

$$\widetilde{\mathbf{W}}(\mathbf{y}) = \rho\omega^2 \int_{\Gamma_0} \Gamma(\mathbf{x}, \mathbf{y}) \overline{\boldsymbol{\xi}}_1(\mathbf{x}) ds(\mathbf{x}) + \rho\omega^2 \int_{\Gamma_0} T_{n_x} \Gamma(\mathbf{x}, \mathbf{y}) \overline{\boldsymbol{\xi}}_2(\mathbf{x}) ds(\mathbf{x}),$$

where $\Gamma(\mathbf{x}, \mathbf{y})$ is the fundamental matrix (see e.g. [17, 34]).

Let $\boldsymbol{\alpha}_1$ and $\boldsymbol{\alpha}_2$ be the extensions of $\overline{\boldsymbol{\xi}}_1$ and $\overline{\boldsymbol{\xi}}_2$ by zero to the whole boundary ∂D . We have

$$\begin{aligned} \widetilde{\mathbf{W}}(\mathbf{y}) &= \rho\omega^2 \int_{\Gamma_0} \Gamma(\mathbf{x}, \mathbf{y}) \overline{\boldsymbol{\xi}}_1(\mathbf{x}) ds(\mathbf{x}) + \rho\omega^2 \int_{\Gamma_0} T_{n_x} \Gamma(\mathbf{x}, \mathbf{y}) \overline{\boldsymbol{\xi}}_2(\mathbf{x}) ds(\mathbf{x}) \\ &= \rho\omega^2 \int_{\partial D} \Gamma(\mathbf{x}, \mathbf{y}) \boldsymbol{\alpha}_1(\mathbf{x}) ds(\mathbf{x}) + \rho\omega^2 \int_{\partial D} T_{n_x} \Gamma(\mathbf{x}, \mathbf{y}) \boldsymbol{\alpha}_2(\mathbf{x}) ds(\mathbf{x}). \end{aligned} \quad (3.22)$$

From the jump relations of single-layer and double-layer potential functions (see e.g. [14, 24, 34]), we can get

$$\widetilde{\mathbf{W}}(\mathbf{y})_+ - \widetilde{\mathbf{W}}(\mathbf{y})_- = \rho\omega^2 \boldsymbol{\alpha}_2, \quad \text{on } \partial D, \quad (3.23)$$

and

$$T_n \widetilde{\mathbf{W}}(\mathbf{y})_- - T_n \widetilde{\mathbf{W}}(\mathbf{y})_+ = \rho\omega^2 \boldsymbol{\alpha}_1, \quad \text{on } \partial D. \quad (3.24)$$

Thus, by the equations (3.21), (3.23) and (3.24), we have

$$\boldsymbol{\alpha}_1 = \boldsymbol{\alpha}_2 = 0.$$

Thus we have

$$\boldsymbol{\xi}_1 = \boldsymbol{\xi}_2 = 0.$$

It means \mathcal{N}^* is injective, and \mathcal{N} has dense range. \square

Remark 3.1. *In practice, given the Cauchy data pair \mathbf{f} and \mathbf{t} , we solve the corresponding ill-posed equations by using regularization methods such as Tikhonov regularization. Since the L^2 -norm is the appropriate norm to measure the data error, it is natural to apply the regularization scheme in the space of square integrable functions. For this reason, we consider the operator $\mathcal{N} : \mathbf{L}^2(\partial B) \rightarrow \mathbf{L}^2(\Gamma_0) \times \mathbf{L}^2(\Gamma_0)$, and theorem 2 is also correct in L^2 -norm*

After this, we write the problem considered in this paper. First, we approximate the solution \mathbf{u} of equation (2.1). In this step, we should find the density function $\boldsymbol{\varphi} \in \mathbf{L}^2(\partial B)$ by

$$\mathcal{N}\boldsymbol{\varphi} = \mathbf{h}, \quad (3.25)$$

here $\mathbf{h} = (\mathbf{f}|_{\Gamma_0}, \mathbf{t}|_{\Gamma_0})^\top$, and then $\mathbf{S}\boldsymbol{\varphi}(x)$ will approximate the displacement \mathbf{u} in D . Second, a Newton type method is used to recover the missing boundary Γ_m and the impedance function χ .

Before giving the uniqueness result, we should first give a property of the solution $\mathbf{u}(\mathbf{x}, \omega)$.

Lemma 3.1. *The displacement $\mathbf{u}(\mathbf{x}, \omega)$ depends analytically on $\omega \in \mathbb{C}$, if $\mathbf{h}(\mathbf{x}, \omega)$ depends analytically on $\omega \in \mathbb{C}$.*

Proof. We seek the displacement field in the form as

$$\mathbf{u}(\mathbf{x}) = \int_{\partial B} \mathbb{E}(\mathbf{x}, \mathbf{y}) \boldsymbol{\varphi}(\mathbf{y}) ds(\mathbf{y}), \quad \mathbf{x} \in D, \quad (3.26)$$

with $\boldsymbol{\varphi} = (\varphi_1, \varphi_2)^\top$ and

$$\mathbb{E}(\mathbf{x}, \mathbf{y}) = \begin{pmatrix} \frac{\partial \Phi(\kappa_p |\mathbf{x}-\mathbf{y}|)}{\partial x_1} & \frac{\partial \Phi(\kappa_s |\mathbf{x}-\mathbf{y}|)}{\partial x_2} \\ \frac{\partial \Phi(\kappa_p |\mathbf{x}-\mathbf{y}|)}{\partial x_2} & -\frac{\partial \Phi(\kappa_s |\mathbf{x}-\mathbf{y}|)}{\partial x_1} \end{pmatrix}.$$

Since the fundamental solution to the Helmholtz equation depends analytically on wavenumber κ_p or κ_s [6], together with $\kappa_p = \omega \sqrt{\frac{\rho}{\lambda+2\mu}}$ and $\kappa_s = \omega \sqrt{\frac{\rho}{\mu}}$, and thus it depends analytically on ω . Since $\mathbf{h}(\mathbf{x}, \omega)$ depends analytically on $\omega \in \mathbb{C}$ and \mathcal{N} has dense range, we know that $\boldsymbol{\varphi}$ depends analytically on $\omega \in \mathbb{C}$. From the above representation (3.26), it can be seen that the displacement field $\mathbf{u}(\mathbf{x}, \omega)$ depends analytically on ω . \square

In the end of this section, we state a uniqueness theorem for the inverse problem under the assumption that we have the knowledge of the Cauchy data pair.

Theorem 3. *Assume that D_1 and D_2 are elastic bodies with impedance χ_1 and χ_2 , respectively, $\partial D_1 \cap \partial D_2 = \Gamma_0$. The corresponding displacements $\mathbf{u}_1(\mathbf{x}, \omega)$, $\mathbf{u}_2(\mathbf{x}, \omega)$ satisfy*

$$\mathbf{u}_1(\mathbf{x}, \omega)|_{\Gamma_0} = \mathbf{u}_2(\mathbf{x}, \omega)|_{\Gamma_0}, \quad T_n \mathbf{u}_1(\mathbf{x}, \omega)|_{\Gamma_0} = T_n \mathbf{u}_2(\mathbf{x}, \omega)|_{\Gamma_0}$$

for the frequency $\omega \in (a, b)$. Then $D_1 = D_2$ and $\chi_1 = \chi_2$.

Proof. Assume that there are two different domains D_1, D_2 with the boundary coefficients χ_1 and χ_2 generating the same Cauchy data pair denoted by (\mathbf{f}, \mathbf{t}) on Γ_0 , $\Gamma_m^{(j)} = \partial D_j \setminus \Gamma_0$. Let $\mathbf{u}_j(\mathbf{x}, \omega), j = 1, 2$ be the solutions

$$\begin{cases} \nabla \cdot \boldsymbol{\sigma}(\mathbf{u}_j) + \rho \omega^2 \mathbf{u}_j = 0, & \text{in } D_j, \\ \mathbf{u}_j = \mathbf{f}(\mathbf{x}, \omega), & \text{on } \Gamma_0, \\ T_{n_j} \mathbf{u}_j + i\omega \chi_j \mathbf{u}_j = 0, & \text{on } \Gamma_m^{(j)}. \end{cases} \quad (3.27)$$

First, we prove $\Gamma_m^{(1)} = \Gamma_m^{(2)}$. It should be noted that $\mathbf{f}(\mathbf{x}, \omega) \neq 0$. Assume on the contradiction that $\Gamma_m^{(1)} \neq \Gamma_m^{(2)}$. Without loss of generality we suppose that there is

a point in $D_1 \setminus \overline{D_2}$. Otherwise we may switch the notations D_1 and D_2 if necessary. Then we can always find a domain $D^* \subset D_1$ such that $\partial D^* = \Lambda_1 \cup \Lambda_2$, $\Lambda_1 \subset \Gamma_m^{(1)}$, $\Lambda_2 \subset \Gamma_m^{(2)}$, $\Lambda_2 \in (\overline{D_1} \cap \overline{D_2})$.

On Λ_1 , we have

$$T_{n_1} \mathbf{u}_1(\mathbf{x}, \omega) = -i\omega \chi_1 \mathbf{u}_1(\mathbf{x}, \omega). \quad (3.28)$$

On Λ_2 , we have

$$T_{n_2} \mathbf{u}_2(\mathbf{x}, \omega) = -i\omega \chi_2 \mathbf{u}_2(\mathbf{x}, \omega). \quad (3.29)$$

Since $\mathbf{u}_1(\mathbf{x}, \omega) = \mathbf{u}_2(\mathbf{x}, \omega)$ on Γ_0 , the uniqueness of the Cauchy problem for elliptic equations will give $\mathbf{u}_1(\mathbf{x}, \omega) = \mathbf{u}_2(\mathbf{x}, \omega)$ in D^* . By $\Lambda_2 \in (\overline{D_1} \cap \overline{D_2})$, we get $\mathbf{u}_1(\mathbf{x}, \omega) = \mathbf{u}_2(\mathbf{x}, \omega)$, and then

$$T_{n_2} \mathbf{u}_1(\mathbf{x}, \omega) = -i\omega \chi_2 \mathbf{u}_1(\mathbf{x}, \omega). \quad (3.30)$$

Let $\boldsymbol{\nu} = -\mathbf{n}_2$, $\chi = -\chi_2$ on Λ_2 and $\boldsymbol{\nu} = \mathbf{n}_1$, $\chi = \chi_1$ on Λ_1 , combining equations (3.28) and (3.30), we have

$$T_{\boldsymbol{\nu}} \mathbf{u}_1(\mathbf{x}, \omega) = -i\omega \chi \mathbf{u}_1(\mathbf{x}, \omega), \quad \text{on } \partial D^*. \quad (3.31)$$

Since $D^* \subset \overline{D_1}$, we know that $u_1(\mathbf{x}, \omega)$ satisfy the Navier equation in D^* with the boundary condition (3.31). The first Betti formula yields

$$\int_{D^*} (E(\mathbf{u}_1, \overline{\mathbf{u}}_1) - \rho\omega^2 |\mathbf{u}_1(\mathbf{x}, \omega)|^2) dx = \int_{\partial D^*} T_{\boldsymbol{\nu}} \mathbf{u}_1(\mathbf{x}, \omega) \cdot \overline{\mathbf{u}}_1(\mathbf{x}, \omega) ds,$$

where

$$\begin{aligned} E(\mathbf{u}_1, \overline{\mathbf{u}}_1) &= \nabla \mathbf{u}_1(\mathbf{x}, \omega) : \mathcal{C} : \nabla \overline{\mathbf{u}}_1(\mathbf{x}, \omega) \\ &= \lambda \operatorname{div} \mathbf{u}_1 \operatorname{div} \overline{\mathbf{u}}_1 + \mu \sum_{p,q=1}^2 \frac{\partial u_p}{\partial x_q} \overline{\left(\frac{\partial u_p}{\partial x_q} + \frac{\partial u_q}{\partial x_p} \right)} \\ &= \lambda |\operatorname{div} \mathbf{u}_1|^2 + 2\mu \left(\left| \frac{\partial u_1}{\partial x_1} \right|^2 + \left| \frac{\partial u_2}{\partial x_2} \right|^2 \right) + \mu \left(\left| \frac{\partial u_1}{\partial x_2} + \frac{\partial u_2}{\partial x_1} \right|^2 \right). \end{aligned} \quad (3.32)$$

Combining the boundary condition (3.31), we have

$$\int_{D^*} (E(\mathbf{u}_1, \overline{\mathbf{u}}_1) - \rho\omega^2 |\mathbf{u}_1(\mathbf{x}, \omega)|^2) dx + i\omega \chi \int_{\partial D^*} |\mathbf{u}_1(\mathbf{x}, \omega)|^2 ds = 0.$$

Taking the real part in the above equation, we have

$$\int_{D^*} (E(\mathbf{u}_1, \overline{\mathbf{u}}_1) - \rho\omega^2 |\mathbf{u}_1(\mathbf{x}, \omega)|^2) dx = 0, \quad \text{for all } \omega \in (a, b). \quad (3.33)$$

The analytical dependance of $u_1(\mathbf{x}, \omega)$ on ω implies that equation (3.33) is valid for $\omega \in \mathbb{C}$.

Now choosing $\omega = 1 + i\delta$ we get $\omega^2 = 1 - \delta^2 + 2i\delta$, then the equation (3.33) will be

$$\int_{D^*} (E(\mathbf{u}_1, \bar{\mathbf{u}}_1) - \rho(1 - \delta^2)|\mathbf{u}_1(\mathbf{x}, \omega)|^2) dx + 2i\rho\delta \int_{D^*} |\mathbf{u}_1(\mathbf{x}, \omega)|^2 dx = 0, \quad (3.34)$$

which implies

$$\rho\delta \int_{D^*} |\mathbf{u}_1(\mathbf{x}, \omega)|^2 dx = 0, \quad \text{for all } \omega = 1 + i\delta, \delta \in \mathbb{R} \quad (3.35)$$

by taking the imaginary part of the equation (3.34). Again using the analytical dependance, we get

$$\mathbf{u}_1(\mathbf{x}, \omega) = 0 \quad \text{in } D^* \quad (3.36)$$

for all $\omega \in \mathbb{C}$. By the uniqueness of the analytic continuation, thus $\mathbf{u}_1(\mathbf{x}, \omega) = 0$ in D_1 for all $\omega \in \mathbb{C}$. This yields

$$\mathbf{f}(\mathbf{x}, \omega) = \mathbf{u}_1(\mathbf{x}, \omega)|_{\Gamma_0} = 0,$$

which contradicts the fact that $\mathbf{f}(\mathbf{x}, \omega) \neq 0$. Hence $\Gamma_m^{(1)} = \Gamma_m^{(2)} = \Gamma_m$, i.e. $D_1 = D_2 = D$.

Next we will check $\chi_1 = \chi_2$. On Γ_0 , we have

$$\mathbf{u}_1(\mathbf{x}, \omega) = \mathbf{u}_2(\mathbf{x}, \omega)$$

and

$$T_n \mathbf{u}_1(\mathbf{x}, \omega) = T_n \mathbf{u}_2(\mathbf{x}, \omega),$$

the uniqueness of the Cauchy problem for elliptic equations will give

$$\mathbf{u}_1(\mathbf{x}, \omega) = \mathbf{u}_2(\mathbf{x}, \omega) \quad \text{in } D. \quad (3.37)$$

Together with $T_n \mathbf{u}_1(\mathbf{x}, \omega) = -i\omega\chi_1 \mathbf{u}_1(\mathbf{x}, \omega)$ and $T_n \mathbf{u}_2(\mathbf{x}, \omega) = -i\omega\chi_2 \mathbf{u}_2(\mathbf{x}, \omega)$ on Γ_m , we have $i\omega\chi_1 \mathbf{u}_1(\mathbf{x}, \omega) = i\omega\chi_2 \mathbf{u}_1(\mathbf{x}, \omega)$, i.e. $i\omega(\chi_1 - \chi_2) \mathbf{u}_1(\mathbf{x}, \omega) = 0$ on Γ_m . If $\mathbf{u}_1(\mathbf{x}, \omega) = 0$ on any open subset $\Gamma \subset \Gamma_m$, we have $T_n \mathbf{u}_1(\mathbf{x}, \omega) = -i\omega\chi_1 \mathbf{u}_1(\mathbf{x}, \omega) = 0$ on Γ . The uniqueness of the Cauchy problem for elliptic equations will give $\mathbf{u}_1(\mathbf{x}, \omega) \equiv 0$ in D . This is a contradiction to the behavior of $\mathbf{u}_1(\mathbf{x}, \omega)$ on Γ_0 with $\mathbf{f}(\mathbf{x}, \omega) \neq 0$. Thus we have $\chi_1 - \chi_2 = 0$ on Γ_m . The proof is completed. \square

4 Recovery method

As discussing in the previous section, we should solve a Cauchy problem first.

4.1 The Cauchy problem

In order to solve the Cauchy problem, we should consider the perturbed equations

$$\mathcal{N}\boldsymbol{\varphi}^\delta = \mathbf{h}^\delta. \quad (4.1)$$

Here, $\mathbf{h}^\delta = (\mathbf{f}^\delta, \mathbf{t}^\delta)^\top \in L^2(\Gamma_0) \times L^2(\Gamma_0)$ is measured noisy data satisfying

$$\|\mathbf{h}^\delta - \mathbf{h}\| \leq \delta \times \|\mathbf{h}\| := \epsilon,$$

where δ is the noise level.

The minimum norm solution (see e.g. [22]) of (3.25) is to solve the following equation

$$\alpha\boldsymbol{\varphi}_\alpha^\delta + \mathcal{N}^*\mathcal{N}\boldsymbol{\varphi}_\alpha^\delta = \mathcal{N}^*\mathbf{h}^\delta, \quad \alpha > 0.$$

and choosing the regularization parameter by Morozov discrepancy principle [36, 38, 39], i.e. via finding the zero of $G(\alpha) := \|\mathcal{N}\boldsymbol{\varphi} - \mathbf{h}^\delta\|^2 - \epsilon^2$. The regularization parameter will be obtained numerically by Newton's method as following:

1. Set $n = 0$, and give an initial regularization parameter $\alpha_0 > 0$.
2. Get $\boldsymbol{\varphi}_{\alpha_n}^\delta$ from $(\alpha_n I + \mathcal{N}^*\mathcal{N})\boldsymbol{\varphi}_{\alpha_n}^\delta = \mathcal{N}^*\mathbf{h}^\delta$.
3. Get $\frac{d}{d\alpha}\boldsymbol{\varphi}_{\alpha_n}^\delta$ from $(\alpha_n I + \mathcal{N}^*\mathcal{N})\frac{d}{d\alpha}\boldsymbol{\varphi}_{\alpha_n}^\delta = -\boldsymbol{\varphi}_{\alpha_n}^\delta$.
4. Get $F(\alpha_n)$ and $F'(\alpha_n)$ by

$$F(\alpha_n) = \|\mathcal{N}\boldsymbol{\varphi}_{\alpha_n}^\delta - \mathbf{h}^\delta\|^2 - \epsilon^2$$

and

$$F'(\alpha_n) = 2\alpha_n \left\| \mathcal{N} \frac{d}{d\alpha} \boldsymbol{\varphi}_{\alpha_n}^\delta \right\|^2 + 2\alpha_n^2 \left\| \frac{d}{d\alpha} \boldsymbol{\varphi}_{\alpha_n}^\delta \right\|^2,$$

respectively.

5. Set $\alpha_{n+1} = \alpha_n - \frac{F(\alpha_n)}{F'(\alpha_n)}$. If $|\alpha_{n+1} - \alpha_n| < \varepsilon$ ($\varepsilon \ll 1$), end. Else, set $n = n + 1$ return to 2.

If the regularization parameter is fixed by α^* , we can achieve the regularized solution $\boldsymbol{\varphi}_{\alpha^*}^\delta = R_{\alpha^*}\mathbf{h}^\delta$ by introducing the regularization operator

$$R_{\alpha^*} := (\alpha^* I + \mathcal{N}^*\mathcal{N})^{-1}\mathcal{N}^*.$$

The displacement \mathbf{u} can be given by $\mathbf{u}^\delta(\mathbf{x}) = \mathcal{S}\boldsymbol{\varphi}_{\alpha^*}^\delta(\mathbf{x})$, which is the treated data in the iterative method.

4.2 Newton-type method

In the above subsection, we have given the approximation of the displacement \mathbf{u} in B by solving equation (4.1), namely $\mathbf{u}^\delta(\mathbf{x})$. Then we can get the gradient explicitly. The gradient of the approximated displacement $\mathbf{u}^\delta(\mathbf{x})$ can be calculated by

$$\nabla \mathbf{u}^\delta(\mathbf{x}) = \int_{\partial B} (\nabla \nabla^\top \Phi(\kappa_p |\mathbf{x} - \mathbf{y}|) \varphi_1(\mathbf{y}) + \nabla \nabla^\perp \Phi(\kappa_s |\mathbf{x} - \mathbf{y}|) \varphi_2(\mathbf{y})) ds(\mathbf{y}). \quad (4.2)$$

Based on the gradient of the approximate scattered field, we are now ready to propose the Newton-type iteration scheme for recovering ∂D and impedance function χ . For a given function \mathbf{g} (\mathbf{g} can be zero) and the approximated displacement $\mathbf{u}^\delta(\mathbf{x})$, we can define the mapping operator \mathcal{F} from the boundary contour γ and impedance function χ to the given function \mathbf{g} by

$$\mathcal{F}(\gamma, \chi) = T_n \mathbf{u}^\delta(\gamma) + i\omega \chi \mathbf{u}^\delta(\gamma).$$

In addition, it should to seek the impedance boundary where the boundary curve γ and impedance function χ satisfy

$$\mathcal{F}(\gamma, \chi) = \mathbf{g}.$$

Our reconstruction algorithm can be summarized as follows:

First, for a given Cauchy data pair (\mathbf{f}, \mathbf{t}) on Γ_0 , we can get the density function φ by

$$\mathcal{N}\varphi(\mathbf{x}) = \mathbf{h}, \quad x \in \Gamma_0. \quad (4.3)$$

Then we can get the treated approximated displacement $\mathbf{u}^\delta(\mathbf{x}) = \mathbf{S}\varphi_{\alpha^*}^\delta(\mathbf{x})$ and traction $\mathbf{t}^\delta(\mathbf{x}) = T_n \mathbf{S}\varphi_{\alpha^*}^\delta(\mathbf{x})$.

Second, for the current approximation to the missing boundary curve $\gamma_n, n = 0, 1, 2, \dots$, and the impedance χ_n we compute $\mathcal{M}_D(\gamma_n) = \mathbf{S}\varphi_{\alpha^*}^\delta(\mathbf{x})|_{\gamma_n}$ and $\mathcal{M}_T(\gamma_n) = T_n \mathbf{S}\varphi_{\alpha^*}^\delta(\mathbf{x})|_{\gamma_n}$. Denote $\mathcal{F} = \mathcal{M}_T + i\omega \chi_n \mathcal{M}_D$ be the combination. We update the boundary curve γ_n via the following procedure

$$\begin{cases} \mathcal{F}(\gamma_n, \chi_n) + \mathcal{F}'(\gamma_n, \chi_n) \Delta \gamma_n = \mathbf{g}, \\ \gamma_{n+1} = \gamma_n + \Delta \gamma_n. \end{cases} \quad (4.4)$$

Third, for the boundary parameterization γ_{n+1} , get the update χ_{n+1} for the impedance function by

$$\begin{cases} \mathcal{F}(\gamma_{n+1}, \chi_n) + i\omega \mathcal{M}_D(\gamma_{n+1}) \Delta \chi_n = \mathbf{g}, \\ \chi_{n+1} = \chi_n + \Delta \chi_n. \end{cases} \quad (4.5)$$

Once we have gotten $\Delta \gamma_n$ and $\Delta \chi_n$, we have updated γ_n and χ_n to γ_{n+1} and χ_{n+1} .

The Fréchet derivatives of $\mathbf{u}^\delta(\mathbf{x})$ and $\mathbf{t}^\delta(\mathbf{x})$ with respect to \mathbf{x} can be calculated by

$$\begin{aligned}\nabla \mathbf{u}^\delta(\mathbf{x}) &= \begin{pmatrix} \partial_{x_1} u_1^\delta & \partial_{x_2} u_1^\delta \\ \partial_{x_1} u_2^\delta & \partial_{x_2} u_2^\delta \end{pmatrix}, \\ \nabla \mathbf{t}^\delta(\mathbf{x}) &= \begin{pmatrix} \partial_{x_1} t_1^\delta & \partial_{x_2} t_1^\delta \\ \partial_{x_1} t_2^\delta & \partial_{x_2} t_2^\delta \end{pmatrix},\end{aligned}$$

where $\varphi_{\alpha^*,1}^\delta$

$$\partial_{x_1} u_1^\delta = \int_{\partial B} (\partial_{x_1} \mathbb{E}_{11}(\mathbf{x}, \mathbf{y}) \varphi_{\alpha^*,1}^\delta(\mathbf{y}) + \partial_{x_1} \mathbb{E}_{12}(\mathbf{x}, \mathbf{y}) \varphi_{\alpha^*,2}^\delta(\mathbf{y})) ds(\mathbf{y}),$$

$$\partial_{x_2} u_1^\delta = \int_{\partial B} (\partial_{x_2} \mathbb{E}_{11}(\mathbf{x}, \mathbf{y}) \varphi_{\alpha^*,1}^\delta(\mathbf{y}) + \partial_{x_2} \mathbb{E}_{12}(\mathbf{x}, \mathbf{y}) \varphi_{\alpha^*,2}^\delta(\mathbf{y})) ds(\mathbf{y}),$$

$$\partial_{x_1} u_2^\delta = \int_{\partial B} (\partial_{x_1} \mathbb{E}_{21}(\mathbf{x}, \mathbf{y}) \varphi_{\alpha^*,1}^\delta(\mathbf{y}) + \partial_{x_1} \mathbb{E}_{22}(\mathbf{x}, \mathbf{y}) \varphi_{\alpha^*,2}^\delta(\mathbf{y})) ds(\mathbf{y}),$$

$$\partial_{x_2} u_2^\delta = \int_{\partial B} (\partial_{x_2} \mathbb{E}_{21}(\mathbf{x}, \mathbf{y}) \varphi_{\alpha^*,1}^\delta(\mathbf{y}) + \partial_{x_2} \mathbb{E}_{22}(\mathbf{x}, \mathbf{y}) \varphi_{\alpha^*,2}^\delta(\mathbf{y})) ds(\mathbf{y}),$$

$$\partial_{x_1} t_1^\delta = \int_{\partial B} \partial_{x_1} \mathbb{T}_{11}(\mathbf{x}, \mathbf{y}) \varphi_{\alpha^*,1}^\delta(\mathbf{y}) + \partial_{x_1} \mathbb{T}_{12}(\mathbf{x}, \mathbf{y}) \varphi_{\alpha^*,2}^\delta(\mathbf{y}) ds(\mathbf{y}),$$

$$\partial_{x_2} t_1^\delta = \int_{\partial B} \partial_{x_2} \mathbb{T}_{11}(\mathbf{x}, \mathbf{y}) \varphi_{\alpha^*,1}^\delta(\mathbf{y}) + \partial_{x_2} \mathbb{T}_{12}(\mathbf{x}, \mathbf{y}) \varphi_{\alpha^*,2}^\delta(\mathbf{y}) ds(\mathbf{y}),$$

$$\partial_{x_1} t_2^\delta = \int_{\partial B} \partial_{x_1} \mathbb{T}_{21}(\mathbf{x}, \mathbf{y}) \varphi_{\alpha^*,1}^\delta(\mathbf{y}) + \partial_{x_1} \mathbb{T}_{22}(\mathbf{x}, \mathbf{y}) \varphi_{\alpha^*,2}^\delta(\mathbf{y}) ds(\mathbf{y}),$$

$$\partial_{x_2} t_2^\delta = \int_{\partial B} \partial_{x_2} \mathbb{T}_{21}(\mathbf{x}, \mathbf{y}) \varphi_{\alpha^*,1}^\delta(\mathbf{y}) + \partial_{x_2} \mathbb{T}_{22}(\mathbf{x}, \mathbf{y}) \varphi_{\alpha^*,2}^\delta(\mathbf{y}) ds(\mathbf{y}).$$

In fact, the forms of the elements $\partial_{x_i} \mathbb{T}_{1j}(\mathbf{x}, \mathbf{y})$ and $\partial_{x_i} \mathbb{T}_{2j}(\mathbf{x}, \mathbf{y})$ are given by

$$\begin{aligned}& \partial_{x_i} \mathbb{T}_{1j}(\mathbf{x}, \mathbf{y}) \\ &= \left[(\lambda + 2\mu) \frac{\partial^2 \mathbb{E}_{1j}(\mathbf{x}, \mathbf{y})}{\partial x_1 \partial x_i} + \lambda \frac{\partial^2 \mathbb{E}_{2j}(\mathbf{x}, \mathbf{y})}{\partial x_2 \partial x_i} \right] n_1(\mathbf{x}) + \mu \left(\frac{\partial^2 \mathbb{E}_{1j}(\mathbf{x}, \mathbf{y})}{\partial x_2 \partial x_i} + \frac{\partial^2 \mathbb{E}_{2j}(\mathbf{x}, \mathbf{y})}{\partial x_1 \partial x_i} \right) n_2(\mathbf{x}) \\ &+ \left[(\lambda + 2\mu) \frac{\partial \mathbb{E}_{1j}(\mathbf{x}, \mathbf{y})}{\partial x_1} + \lambda \frac{\partial \mathbb{E}_{2j}(\mathbf{x}, \mathbf{y})}{\partial x_2} \right] \frac{\partial n_1(\mathbf{x})}{\partial x_i} + \mu \left(\frac{\partial \mathbb{E}_{1j}(\mathbf{x}, \mathbf{y})}{\partial x_2} + \frac{\partial \mathbb{E}_{2j}(\mathbf{x}, \mathbf{y})}{\partial x_1} \right) \frac{\partial n_2(\mathbf{x})}{\partial x_i}.\end{aligned}$$

$$\begin{aligned}& \partial_{x_i} \mathbb{T}_{2j}(\mathbf{x}, \mathbf{y}) \\ &= \mu \left(\frac{\partial^2 \mathbb{E}_{1j}(\mathbf{x}, \mathbf{y})}{\partial x_2 \partial x_i} + \frac{\partial^2 \mathbb{E}_{2j}(\mathbf{x}, \mathbf{y})}{\partial x_1 \partial x_i} \right) n_1(\mathbf{x}) + \left[\lambda \frac{\partial^2 \mathbb{E}_{1j}(\mathbf{x}, \mathbf{y})}{\partial x_1 \partial x_i} + (\lambda + 2\mu) \frac{\partial^2 \mathbb{E}_{2j}(\mathbf{x}, \mathbf{y})}{\partial x_2 \partial x_i} \right] n_2(\mathbf{x}) \\ &+ \mu \left(\frac{\partial \mathbb{E}_{1j}(\mathbf{x}, \mathbf{y})}{\partial x_2} + \frac{\partial \mathbb{E}_{2j}(\mathbf{x}, \mathbf{y})}{\partial x_1} \right) \frac{\partial n_1(\mathbf{x})}{\partial x_i} + \left[\lambda \frac{\partial \mathbb{E}_{1j}(\mathbf{x}, \mathbf{y})}{\partial x_1} + (\lambda + 2\mu) \frac{\partial \mathbb{E}_{2j}(\mathbf{x}, \mathbf{y})}{\partial x_2} \right] \frac{\partial n_2(\mathbf{x})}{\partial x_i}.\end{aligned}$$

For this iterative algorithm, we have to create a stopping criterion. For convenience, the stopping of the iterative process we perform with the following relative error

$$E_n = \frac{\|\Delta\gamma_n\|_{L^2}}{\|\gamma_{n-1}\|_{L^2}} + \frac{\|\Delta\chi_n\|_{L^2}}{\|\chi_{n-1}\|_{L^2}}. \quad (4.6)$$

We choose a constant $\varepsilon > 0$. If $E_n > \varepsilon$, the iteration process is continued. Otherwise, it is stopped.

For the sake of simplicity, we assume that the boundary is starlike with respect to the origin, i.e. ∂D can be represented in the parametric form

$$\partial D = \{r(\vartheta)(\cos \vartheta, \sin \vartheta), \vartheta \in [0, 2\pi)\}$$

where $r : R \rightarrow R$ is a positive, twice continuously differentiable and 2π -periodic function. In this paper we assume that

$$\Gamma_0 = \{r(\vartheta)(\cos \vartheta, \sin \vartheta), \vartheta \in [0, \pi)\}$$

as the known part coincides with the measured Cauchy data and

$$\Gamma_m = \{r(\vartheta)(\cos \vartheta, \sin \vartheta), \vartheta \in [\pi, 2\pi)\}$$

as the missing part of the boundary with the absorbing boundary condition.

To numerically approximate $r(\vartheta)$, we assume that $r(\vartheta)$ is represented as the trigonometric polynomials of degree less than or equal to N , namely

$$r(\vartheta) = a_0 + \sum_{j=1}^N (a_j \cos j\vartheta + b_j \sin j\vartheta). \quad (4.7)$$

In the n -th iterative step, the radial function r_n will be updated to the r_{n+1} by Δr_n . This process will be achieved by updating the Fourier coefficients $\mathbf{a} = (a_0, a_1, \dots, a_N, b_1, \dots, b_N)^\top$. If we remember $\mathbf{a}^{(n)} = (a_0^{(n)}, a_1^{(n)}, \dots, a_N^{(n)}, b_1^{(n)}, \dots, b_N^{(n)})^\top$ be the Fourier coefficients in the n -th step, then the Fourier coefficients in iterative process **step 2** will be updated by $\mathbf{a}^{(n+1)} = \mathbf{a}^{(n)} + \Delta \mathbf{a}^{(n)}$ by the following procedure

$$\begin{cases} \mathbf{t}^\delta(A\mathbf{a}^{(n)}\hat{x}) + i\omega\chi_n \mathbf{u}^\delta(A\mathbf{a}^{(n)}\hat{x}) + \nabla (\mathbf{t}^\delta(A\mathbf{a}^{(n)}\hat{x}) + i\omega\chi_n \mathbf{u}^\delta(A\mathbf{a}^{(n)}\hat{x})) (A\Delta \mathbf{a}^{(n)}) \hat{x} = \mathbf{g}(A\mathbf{a}^{(n)}\hat{x}), \\ \mathbf{a}^{(n+1)} = \mathbf{a}^{(n)} + \Delta \mathbf{a}^{(n)}, \end{cases}$$

where $\hat{x} = (\cos \vartheta, \sin \vartheta)^\top$ and $A = (1, \cos \vartheta, \dots, \cos N\vartheta, \sin \vartheta, \dots, \sin N\vartheta)$.

Whilst the update impedance function χ_{n+1} in iterative process **step 3** will be as following

$$\begin{cases} \mathbf{t}^\delta(A\mathbf{a}^{(n+1)}\hat{x}) + i\omega\chi_n \mathbf{u}^\delta(A\mathbf{a}^{(n+1)}\hat{x}) + i\omega \mathbf{u}^\delta(A\mathbf{a}^{(n+1)}\hat{x}) \Delta \chi_n = \mathbf{g}(A\mathbf{a}^{(n+1)}\hat{x}), \\ \chi_{n+1} = \chi_n + \Delta \chi_n. \end{cases} \quad (4.8)$$

For convenience, the stopping rule will be replaced by the following relative error

$$E_n = \frac{\|\Delta \mathbf{a}^{(n)}\|_{L^2}}{\|\mathbf{a}^{(n-1)}\|_{L^2}} + \frac{\|\Delta \chi_n\|_{L^2}}{\|\chi_{n-1}\|_{L^2}}. \quad (4.9)$$

We choose a constant $\varepsilon > 0$. If $E_n > \varepsilon$, the iteration process is continued. Otherwise, it is stopped.

5 Numerical Examples

In this part, we will give some examples to show the effectiveness of the present method. The Lemé constants λ and μ are given by $\lambda = 1$ and $\mu = 1$. The inside of the elastic obstacle is assumed to be filled with a homogeneous and isotropic elastic medium with a unit mass, i.e. $\rho = 1$. The wavenumbers κ_p and κ_s are usually determined by the relationship between the wavenumbers and the Lemé constants $\kappa_p = \sqrt{\frac{\rho\omega^2}{\lambda+2\mu}}$ and $\kappa_s = \sqrt{\frac{\rho\omega^2}{\mu}}$. The initial guess of the boundary is a half circle, and the initial guess of the impedance function is a constant function. The number of the coefficients is 17, i.e. $N = 8$ in equation (4.7).

In the practice, we know all the information of the known part including the Cauchy data pair (\mathbf{f}, \mathbf{t}) about Γ_0 . And we can easily get the equation $T_n \mathbf{u} + i\omega\chi \mathbf{u} = \mathbf{g}$ on Γ_0 . Thus we can deal with iterative procedure on the whole boundary ∂D . The initial guess of the boundary is a circle. The results about the known part can give a reference result for the present method.

Example 5.1. *In this example, D is a apple-shaped domain, and the boundary ∂D be*

$$\mathbf{z}(\vartheta) = \frac{1 + 0.8 \cos \vartheta + 0.2 \sin 2\vartheta}{1 + 0.7 \cos \vartheta} (\cos \vartheta, \sin \vartheta)$$

with the parameterized surface impedance χ given by $\chi(\vartheta) = \sin^4 \vartheta$, $\vartheta \in [\pi, 2\pi)$. The components u_p and u_s of the displacement \mathbf{u} inside the elastic obstacle are generated by

$$u_p(\mathbf{x}) = J_0^{(1)}(\kappa_p |\mathbf{x} - \mathbf{y}_0|), \quad u_s(\mathbf{x}) = J_0^{(1)}(\kappa_s |\mathbf{x} - \mathbf{y}_0|), \quad \mathbf{x} \in \overline{D},$$

where $\mathbf{y}_0 = (1, 0)$, i.e. $\mathbf{u}(\mathbf{x}) = \nabla u_p(\mathbf{x}) + \nabla^\perp u_s(\mathbf{x})$. We fix the frequency by $\omega = 3$. The so called virtual boundary ∂B is a circle, and its radius is 4. The initial guess of the boundary is a circle, and its radius is 0.3. Figure 1 shows the numerical reconstructions of the missing boundary and the impedance function with different noise levels $\delta \in \{0\%, 1\%, 5\%\}$ for Example 5.1. We can see that the numerical reconstructions are satisfactory. The reconstruction improves as the noise decreases.

Example 5.2. *The components u_p and u_s of the displacement \mathbf{u} inside the elastic obstacle are generated by*

$$u_p(\mathbf{x}) = \frac{i}{4} H_0^{(1)}(\kappa_p |\mathbf{x} - \mathbf{y}_0|), \quad u_s(\mathbf{x}) = \frac{i}{4} H_0^{(1)}(\kappa_s |\mathbf{x} - \mathbf{y}_0|), \quad \mathbf{x} \in \overline{D},$$

i.e. $\mathbf{u}(\mathbf{x}) = \nabla u_p(\mathbf{x}) + \nabla^\perp u_s(\mathbf{x})$. The so called virtual boundary ∂B is a circle, and its radius is 4. The initial guess of the boundary is a circle as in Example 5.1.

First, D is a peanut-shaped domain, and the boundary ∂D be

$$\mathbf{z}(\vartheta) = R_0 (4 \cos^2 \vartheta + \sin^2 \vartheta)^{\frac{1}{2}} (\cos \vartheta, \sin \vartheta)$$

Table 1: The iterative steps and the regularization parameter.

Noise level	Iterative steps	Regularization parameter
0%	127	1.2019e-13
1%	128	9.7500e-02
5%	147	2.5117e-00

with $R_0 = 0.5$. We fix the frequency by $\omega = 5$, $\mathbf{y}_0 = (4, -9)$. The parameterized surface impedance χ is given by

$$\chi(\vartheta) = \sin^4 \vartheta, \vartheta \in [\pi, 2\pi).$$

Second, D is a starfish-shaped domain, and the boundary ∂D be

$$\mathbf{z}(\vartheta) = (1 + 0.2 \cos 5\vartheta) (\cos \vartheta, \sin \vartheta).$$

We fix the frequency by $\omega = 3$, $\mathbf{y}_0 = (4, 9)$. The parameterized surface impedance χ is given by a constant function

$$\chi(\vartheta) = 1, \vartheta \in [\pi, 2\pi).$$

Table 2: The iterative steps and the regularization parameter.

Noise level	Iterative steps	Regularization parameter
0%	88	8.2341e-13
1%	98	2.5200e-02
5%	76	0.3063e-00

Figures 2 and 3 show the numerical reconstructions of the missing boundary and the impedance function with different noise levels $\delta \in \{0\%, 1\%, 5\%\}$ for the first and second case. We can see that the impedance function χ is sensitive depending on the noise level either for a function or for a constant function. The numerical reconstructions of the missing boundary are satisfactory. From table 1 and 2, we can also see that the number of the iterative steps using the noise data are not much more than using the exact data.

Example 5.3. *In this example, we consider D be a circle, and its radius is 1.2. Consider the following boundary value problem*

$$\begin{cases} \Delta u_p + \kappa_p^2 u_p = 0, & \text{in } D, \\ \Delta u_s + \kappa_s^2 u_s = 0, & \text{in } D, \\ T_n \mathbf{u} + i\omega \chi \mathbf{u} = \mathbf{g}, & \text{on } \partial D. \end{cases} \quad (5.1)$$

The impedance function χ is given by

$$\chi(\vartheta) = \sin^2 \vartheta, \quad \vartheta \in [0, 2\pi), \quad (5.2)$$

and the input boundary function $\mathbf{g}(\mathbf{x}) = (g_1, g_2)^\top$ is

$$g_1(\mathbf{x}(\vartheta)) = g_2(\mathbf{x}(\vartheta)) = \sin^2 \vartheta, \quad \vartheta \in [0, 2\pi). \quad (5.3)$$

In order to solve the inverse problem, we first get the Cauchy data $\mathbf{f} = \mathbf{u}|_{\Gamma_0}$ and $\mathbf{t} = T_n \mathbf{u}|_{\Gamma_0}$ by solving the direct problem (5.1). In this step, we use $\partial B = \{\mathbf{x} : |\mathbf{x}| = 3\}$. After this we use $\partial B = \{\mathbf{x} : |\mathbf{x}| = 7\}$ for solving the inverse problem. The initial guess of the boundary is a circle, and its radius is 0.6. The initial guess of the impedance function is a constant function $\chi_0 = 0.5$.

We fix the frequency by $\omega = 2$. The iterative steps and the regularization parameter chosen by Morozov discrepancy principle are given in Table 3. Figure 4 shows the numerical reconstructions of the missing boundary and the impedance function with different noise levels $\delta \in \{0\%, 1\%, 5\%\}$ for Example 5.3. We can see that the numerical reconstructions are satisfactory. From Table 3, we can also see that the number of the iterative steps using the noise data are not much more than using the exact data.

Table 3: The iterative steps and the regularization parameter.

Noise level	Iterative steps	Regularization parameter
0%	44	9.8186e-17
1%	47	1.0717e-05
5%	50	8.4172e-05

Example 5.4. As in example 5.3, we consider the same impedance boundary value problem. Different from the example 5.3, D is a peanut-shaped domain, and the boundary ∂D be

$$\mathbf{z}(\vartheta) = 0.5 (4 \cos^2 \vartheta + \sin^2 \vartheta)^{\frac{1}{2}} (\cos \vartheta, \sin \vartheta).$$

The initial guess of the boundary is a circle, and its radius is 0.3. The initial guess of the impedance function is a constant function $\chi_0 = 1$. We fix the frequency by $\omega = 1$. The iterative steps and the regularization parameter chosen by Morozov discrepancy principle are given in Table 4. Figure 5 shows the numerical reconstructions of the missing boundary and the impedance function with different noise levels $\delta \in \{0\%, 1\%, 5\%\}$ for Example 5.4. We can see that the numerical reconstructions are satisfactory. From Table 4, we can also see that the number of the iterative steps using the noise data are not much more than using the exact data.

Table 4: The iterative steps and the regularization parameter.

Noise level	Iterative steps	Regularization parameter
0%	11	1.5751e−15
1%	12	1.1075e−11
5%	13	2.2101e−10

6 Concluding remarks

In this paper, we have studied the inverse elastic problem by a Newton-type iterative algorithm. This present problem is divided into two parts. The first part is to solve a Cauchy problem through using an indirect integral equation method combining a regularization technique. The second part is simultaneously to recover the elastic impedance and the shape by a Newton-type iterative method. The effectiveness of the method has been shown by solving some examples. In the numerical examples, we construct the exact solution of the scattered field of the displacement to check the feasibility and accuracy of the presented method.

Acknowledgements

The research was supported by the Natural Science Foundation of China (No: 11501566), the Fundamental Research Funds for the Central Universities (No. 3122019159) and Tianjin Education Commission Research Project (No: 2022KJ072).

ORCID ID

Yao Sun: <https://orcid.org/0009-0005-0639-6071>

Declarations

Conflict of interest: The authors declare that they have no conflict of interest.

Data availability: The datasets generated during the current study are available on reasonable request.

References

- [1] G. Alessandrini, A. Morassi and E. Rosset, Detecting cavities by electrostatic boundary measurements. *Inverse Problems*, 18(5):1333, 2002.

- [2] C. Alves and R. Kress, On the far-field operator in elastic obstacle scattering. *IMA Journal of Applied Mathematics*, 67:1–21, 2002.
- [3] H. Ammari, E. Bretin, J. Garnier, H. Kang, H. Lee and A. Wahab, In *Mathematical Methods in Elasticity Imaging*. Princeton University Press, 04 2015.
- [4] H. Ammari, E. Bretin, J. Garnier, H. Kang, H. Lee and A. Wahab, In *Theory of Elasticity*. 1986.
- [5] S. Andrieux, T. N. Baranger and A. B. Abda, Solving cauchy problems by minimizing an energy-like functional. *Inverse Problems*, 22:115 – 133, 2006.
- [6] D. Colton and R. Kress, *Inverse Acoustic and Electromagnetic Scattering Theory*, 4th edn (New York: Springer), 2019.
- [7] F. Cakoni and R. Kress, Integral equations for inverse problems in corrosion detection from partial cauchy data. *Inverse Problems and Imaging*, 1:229–245, 2007.
- [8] F. Cakoni, R. Kress and C. Schuft, Simultaneous reconstruction of shape and impedance in corrosion detection. *Methods and Applications of Analysis*, 17, 2010.
- [9] Y. Chang, Y. Guo, H. Liu, D. Zhang, Recovering source location, polarization, and shape of obstacle from elastic scattering data, *Journal of Computational Physics*, 489:112289, 2023.
- [10] P. Deuffhard, H. W. Engl and O. Scherzer, A convergence analysis of iterative methods for the solution of nonlinear ill-posed problems under affinity invariant conditions. *Inverse Problems*, 14(5):1081, 1998.
- [11] H. W. Engl, M. Hanke and A. Neubauer. Regularization of inverse problems. 1996.
- [12] J. Elschner and M. Yamamoto, Uniqueness in inverse elastic scattering with finitely many incident waves. *Inverse Problems*, 26(4):045005, 2010.
- [13] D. Fasino and G. Inglese, Discrete methods in the study of an inverse problem for Laplace’s equation. *IMA Journal of Numerical Analysis*, 19(1):105–118, 1999.
- [14] S.N. Fata, B.B. Guzina, A linear sampling method for near-field inverse problems in elastodynamics. *Inverse Problems*, 20:713–736, 2004.
- [15] S.N. Fata, B.B. Guzina, Elastic scatterer reconstruction via the adjoint sampling method. *SIAM Journal on Applied Mathematics*, 67(5):1330–1352, 2007.

- [16] T. Hohage, *Iterative Methods in Inverse Obstacle Scattering: Regularization Theory of Linear and Nonlinear Exponentially Ill-Posed Problems*. PhD thesis, 1999
- [17] G. Hu, A. Kirsch and M. Sini, Some inverse problems arising from elastic scattering by rigid obstacles. *Inverse Problems*, 29(1):015009, 2013.
- [18] G. Hu, A. Mantile, M. Sini and T. Yin, Direct and inverse time-harmonic elastic scattering from point-like and extended obstacles. *Inverse Problems and Imaging*, 14(6):1025–1056, 2020.
- [19] P. Jakubik and R. Potthast, Testing the integrity of some cavity –the cauchy problem and the range test. *Applied Numerical Mathematics*, 58(6):899–914, 2008.
- [20] A. Karageorghis, D. Lesnic, L. Marin, The method of fundamental solutions for the identification of a scatterer with impedance boundary condition in interior inverse acoustic scattering. *Eng. Anal. Bound. Elem.* 92: 218–224, 2018.
- [21] A. Karageorghis, B.T. Johansson, D. Lesnic, The method of fundamental solutions for the identification of a sound-soft obstacle in inverse acoustic scattering. *Appl. Numer. Math.* 62(12):1767–1780, 2012.
- [22] R. Kress, *Linear Integral Equations*, Springer-Verlag, Berlin, 1989.
- [23] R. Kress, Uniqueness and numerical methods in inverse obstacle scattering. *Journal of Physics: Conference Series*, 73(1):012003, 2007.
- [24] V.D. Kupradze, *Three-dimensional problems of the mathematical theory of elasticity and thermoelasticity*. Amsterdam: North-Holland; 1979.
- [25] R. Kress, W. Rundell, Inverse scattering for shape and impedance. *Inverse Problems*, 17(4): 1075–1085, 2001.
- [26] R. Kress and W. Rundell, Nonlinear integral equations and the iterative solution for an inverse boundary value problem. *Inverse Problems*, 21(4):1207, 2005.
- [27] R. Kress, W. Rundell, Inverse scattering for shape and impedance revisited. *Journal of Integral Equations and Applications*, 30(2):293–311, 2018.
- [28] P. Li, Y. Wang, Y. Zhao, Near-field imaging of biperiodic surfaces for elastic waves. *Journal of Computational Physics*, 324: 1-23, 2016.
- [29] X. Liu, J. Sun, Data recovery in inverse scattering: From limited-aperture to full-aperture. *Journal of Computational Physics*, 386:350-364, 2019.

- [30] Y. Liu, W. Jiang J. Yang, G. Li, The application of elastic impedance inversion in reservoir prediction at the jinan area of tarim oilfield. *Applied Geophysics*, pages 201–206, 2007.
- [31] J. Liu, X. Liu, J. Sun, Extended sampling method for inverse elastic scattering problems using one incident wave. *SIAM Journal on Imaging Sciences*, 12(2):874–892, 2019.
- [32] F.L. Louër, On the fréchet derivative in elastic obstacle scattering. *SIAM Journal on Applied Mathematics*, 72(5):1493–1507, 2012.
- [33] F. L. Louër, A domain derivative-based method for solving elastodynamic inverse obstacle scattering problems. *Inverse Problems*, 31(11):115006, 2015.
- [34] W. McLean, *Strongly Elliptic Systems and Boundary Integral Equations*, Cambridge: Cambridge University Press, 2000.
- [35] A. Morassi and E. Rosset, Stable determination of cavities in elastic bodies. *Inverse Problems*, 20(2):453, 2004.
- [36] Y. Sun, F. Ma, D. Zhang, An integral equations method combined minimum norm solution for 3D elastostatics Cauchy problem. *Computer Methods in Applied Mechanics and Engineering*, 271: 231–252, 2014.
- [37] Y. Sun. Indirect boundary integral equation method for the cauchy problem of the laplace equation. *Journal of Scientific Computing*, 71(2):469–498, 2017.
- [38] Y. Sun, L. Marin, An invariant method of fundamental solutions for two-dimensional isotropic linear elasticity. *International Journal of Solids and Structures*, 117: 191–207, 2017.
- [39] Y. Sun, F. Ma, X. Zhou, An Invariant Method of Fundamental Solutions for the Cauchy Problem in Two-Dimensional Isotropic Linear Elasticity. *Journal of Scientific Computing*, 64: 197–215, 2015.
- [40] Y. Sun, L. He, B. Chen, Application of neural networks to inverse elastic scattering problems with near-field measurements. *Electronic Research Archive*, 31(11): 7000–7020, 2023.
- [41] Y. Sun, Y. Wang, A highly accurate indirect boundary integral equation solution for three dimensional elastic scattering problem. *Eng. Anal. Bound. Elem.* 159: 402–417, 2024.
- [42] J. Zhang, Y. Wang, B. Xu, Q. Zhen and Y. Wu, Elastic impedance inversion based on improved particle swarm optimization. *Journal of Physics: Conference Series*, 1069(1):012042, 2018.

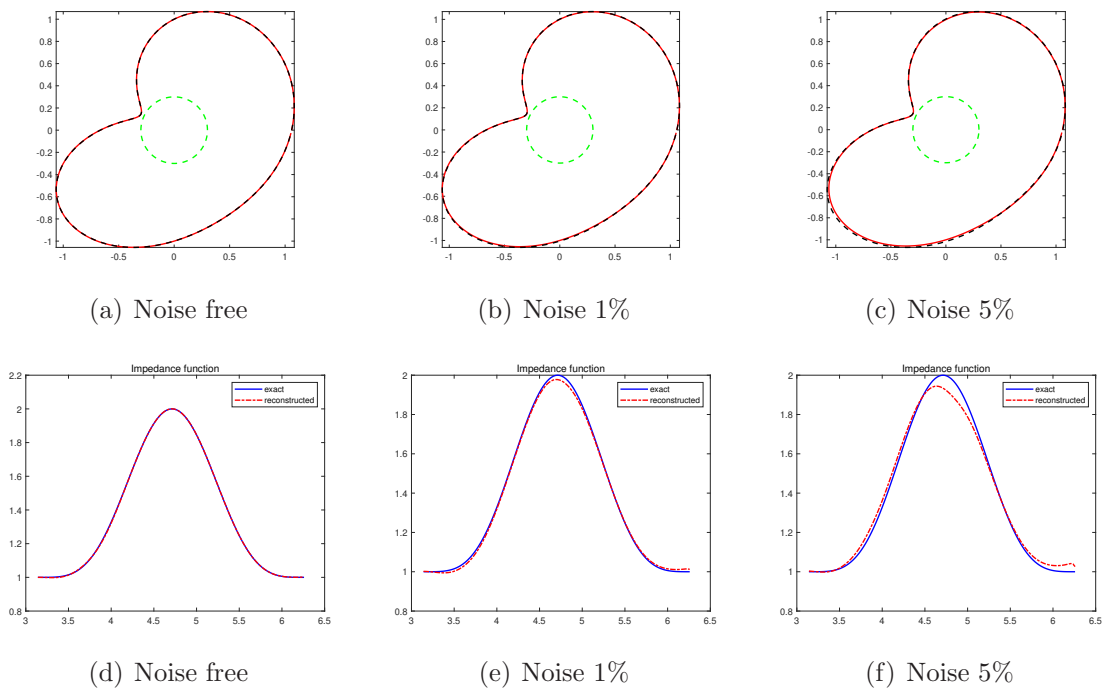


Figure 1: The numerical reconstructions of the shape and the impedance function with different noise levels $\delta \in \{0\%, 1\%, 5\%\}$ in Example 5.1.

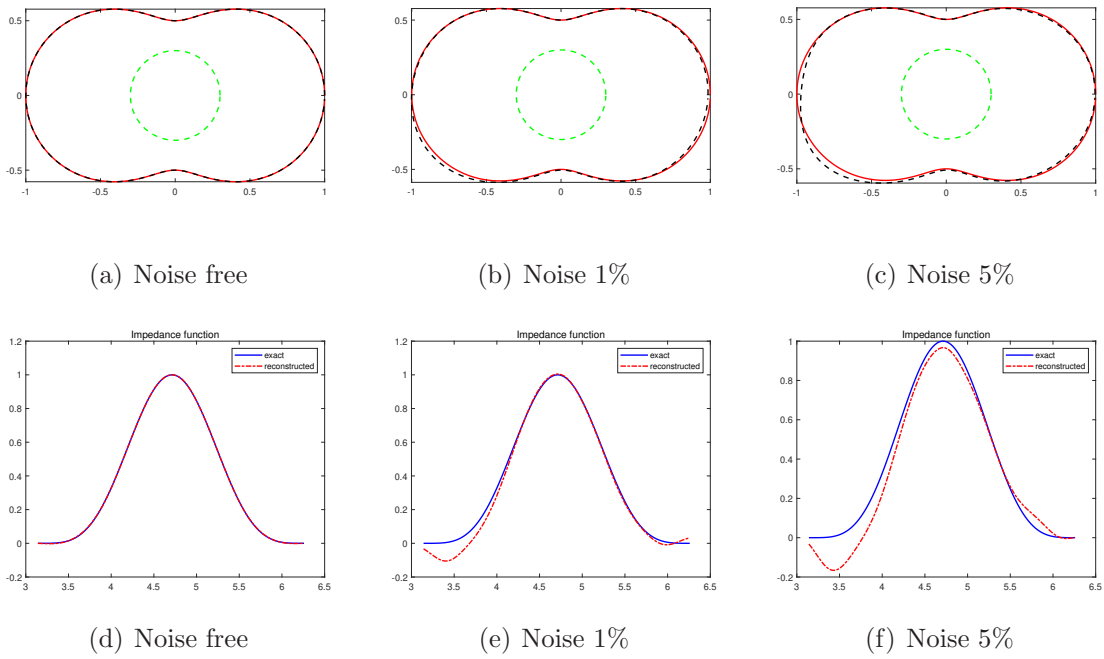


Figure 2: The numerical reconstructions of the shape and the impedance function with different noise levels $\delta \in \{0\%, 1\%, 5\%\}$ for peanut-shaped domain in Example 5.2.

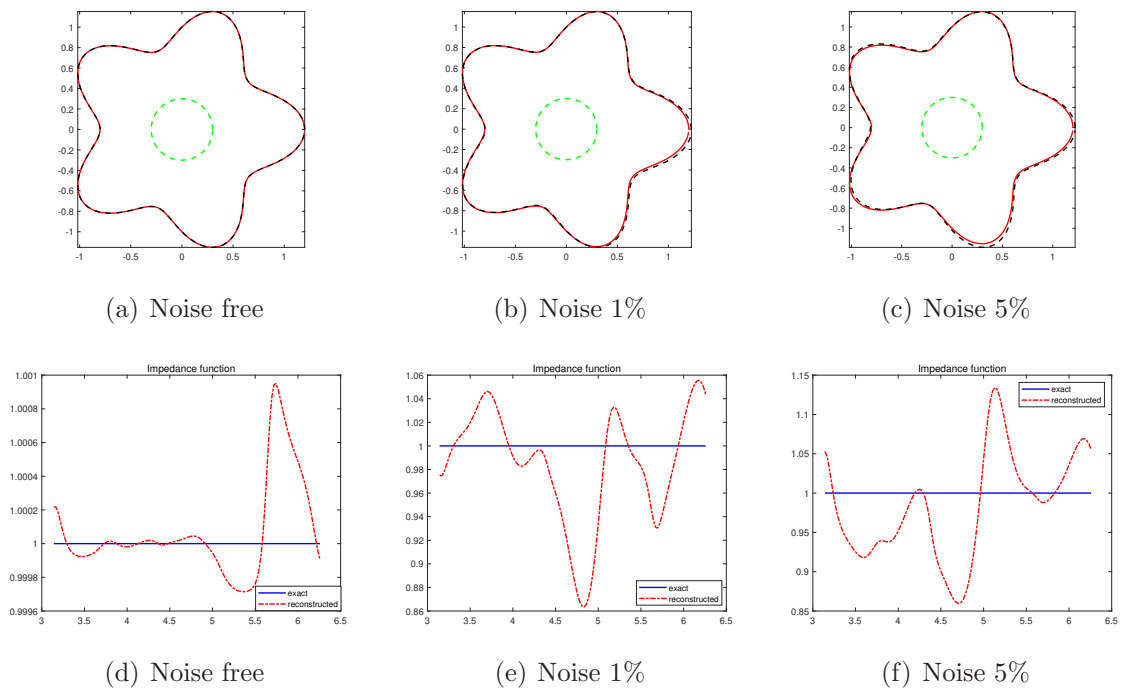


Figure 3: The numerical reconstructions of the shape and the impedance function with different noise levels $\delta \in \{0\%, 1\%, 5\%\}$ for the starfish-shaped domain in Example 5.2.

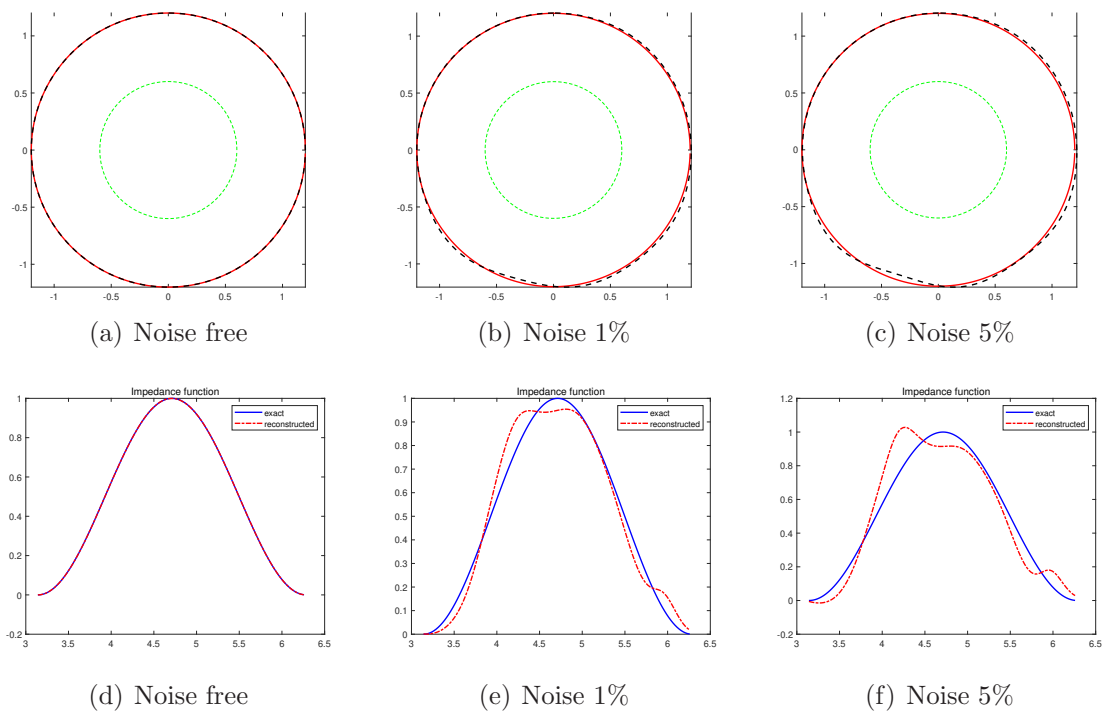


Figure 4: The numerical reconstructions of the shape and the impedance function with different noise levels $\delta \in \{0\%, 1\%, 5\%\}$ in Example 5.3.

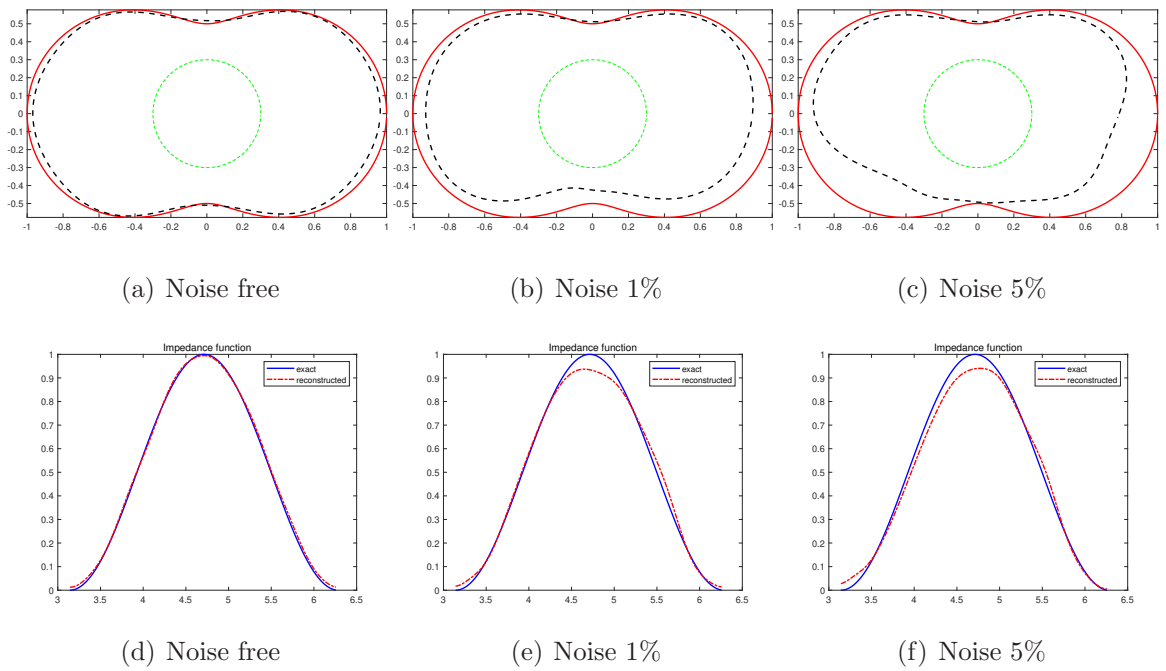
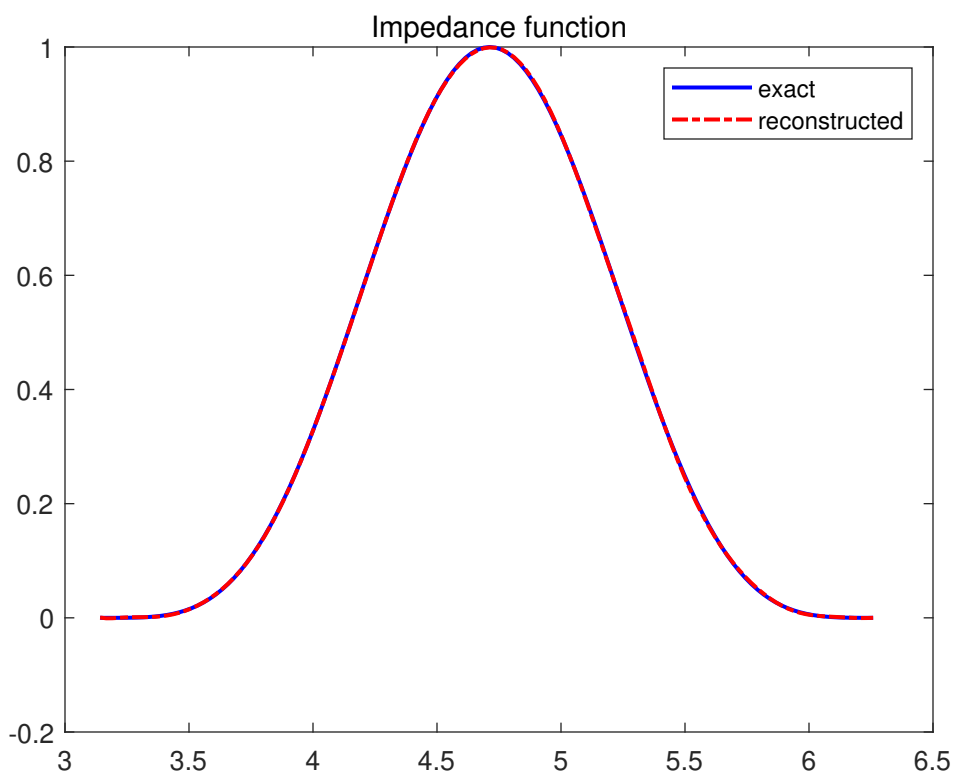
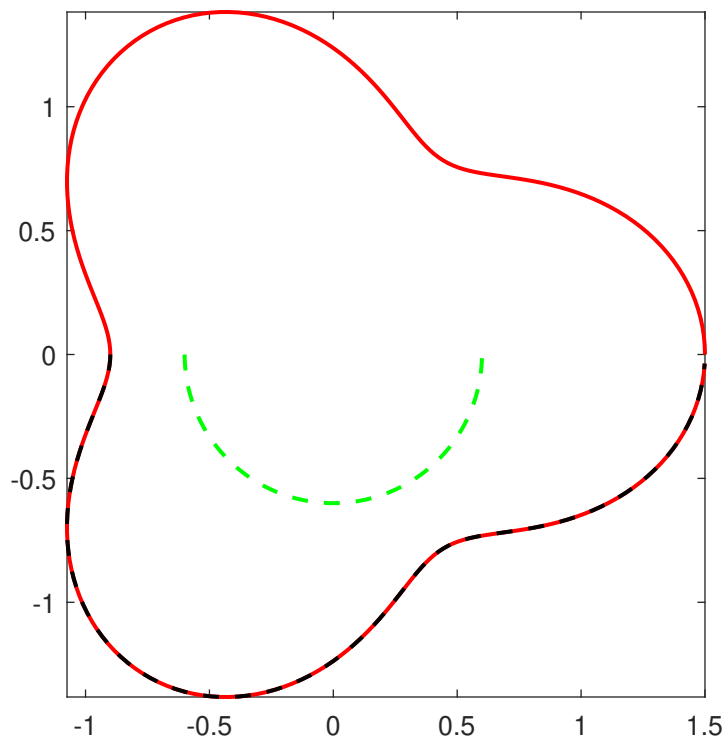
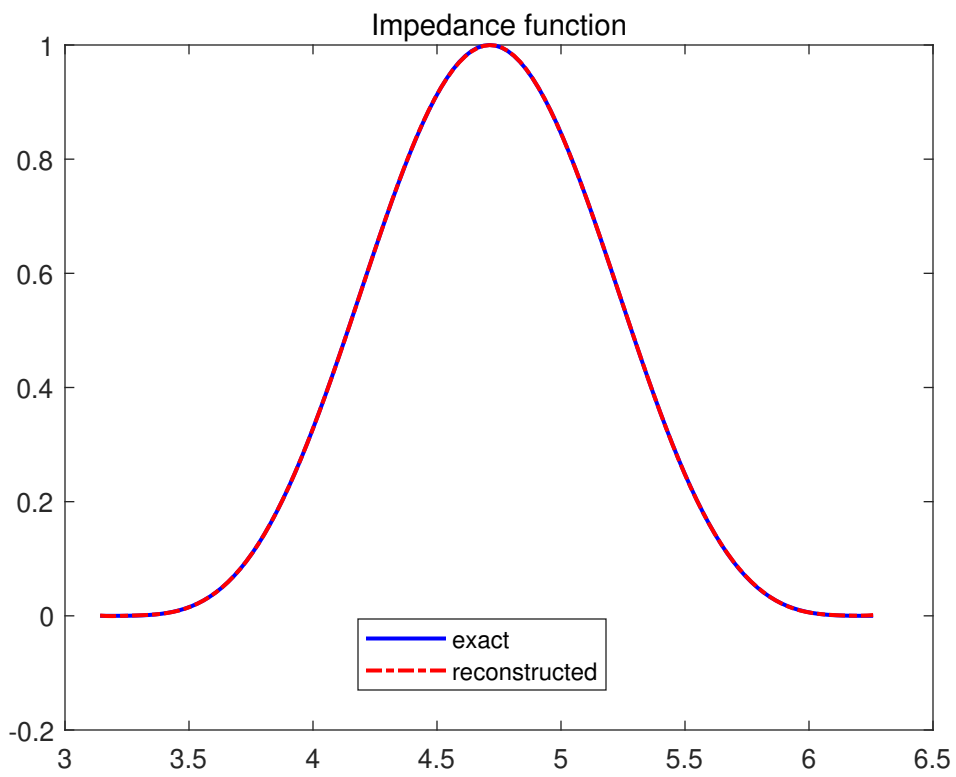
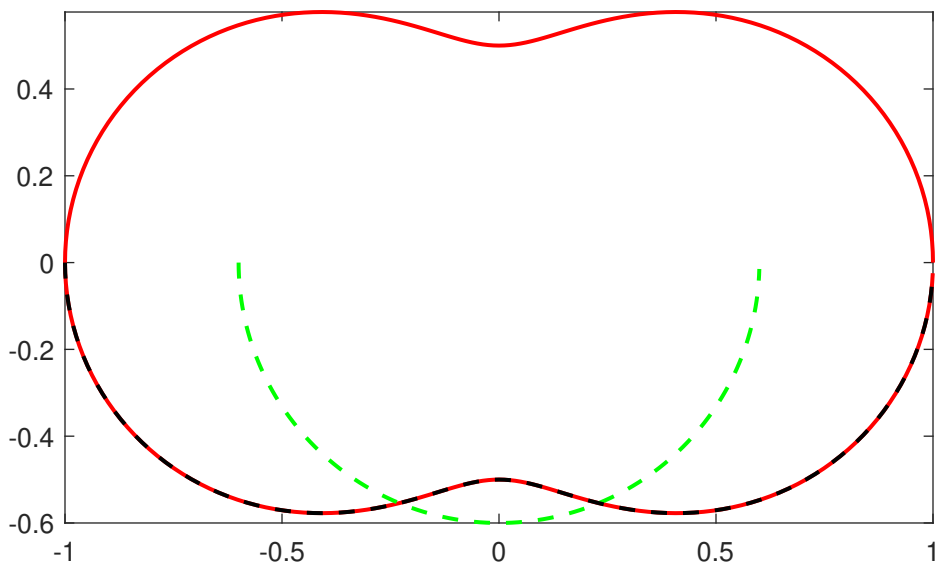


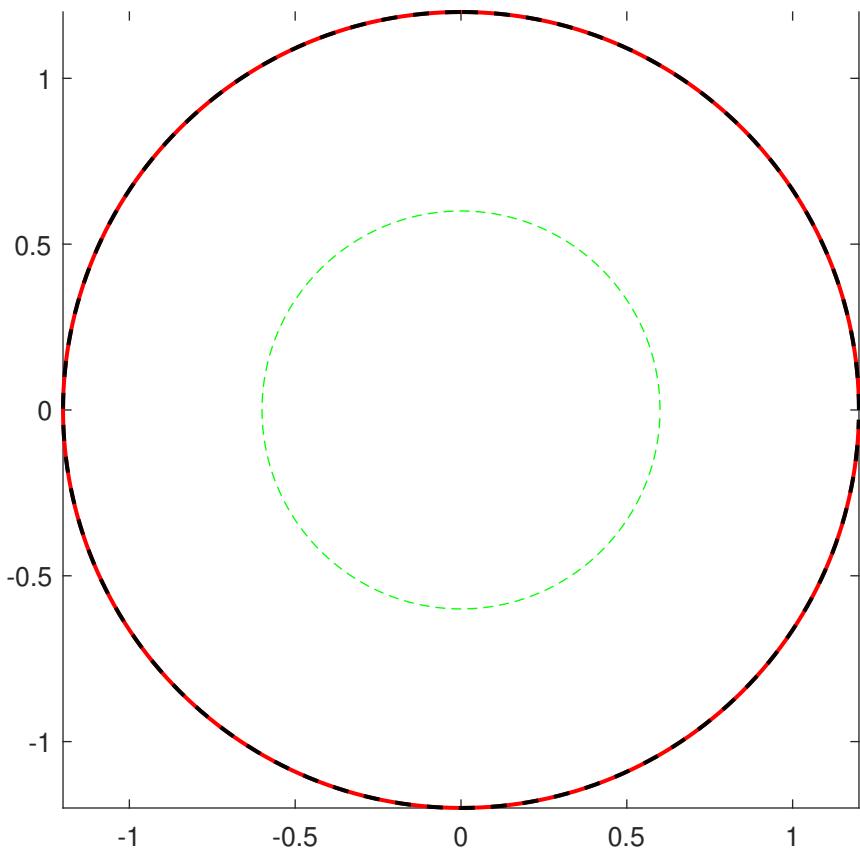
Figure 5: The numerical reconstructions of the shape and the impedance function with different noise levels $\delta \in \{0\%, 1\%, 5\%\}$ in Example 5.4.

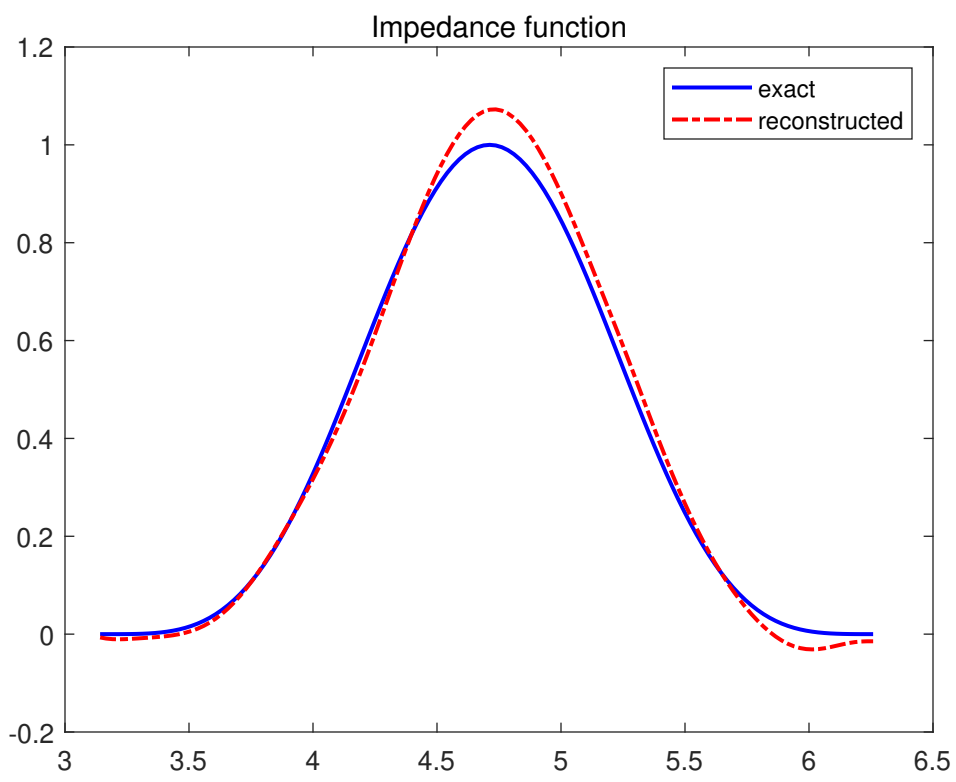


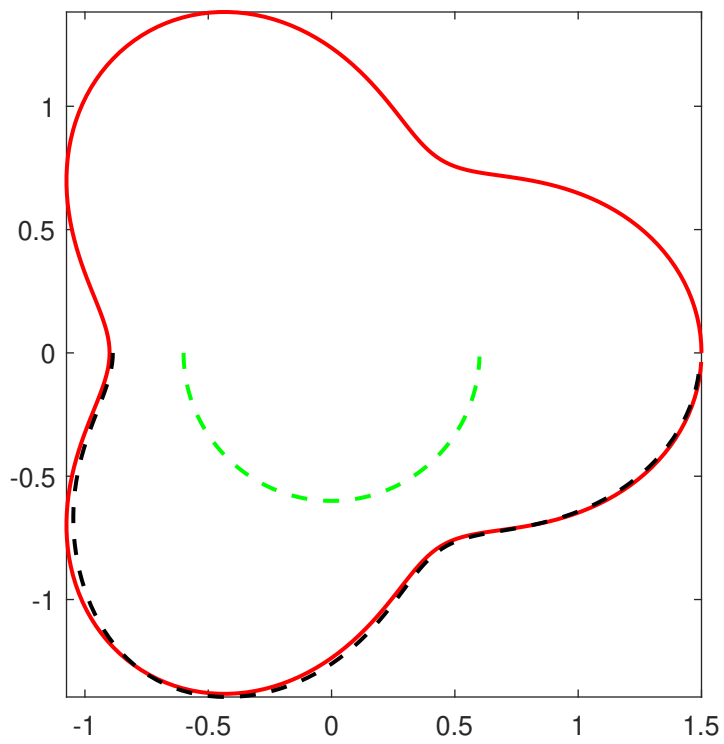


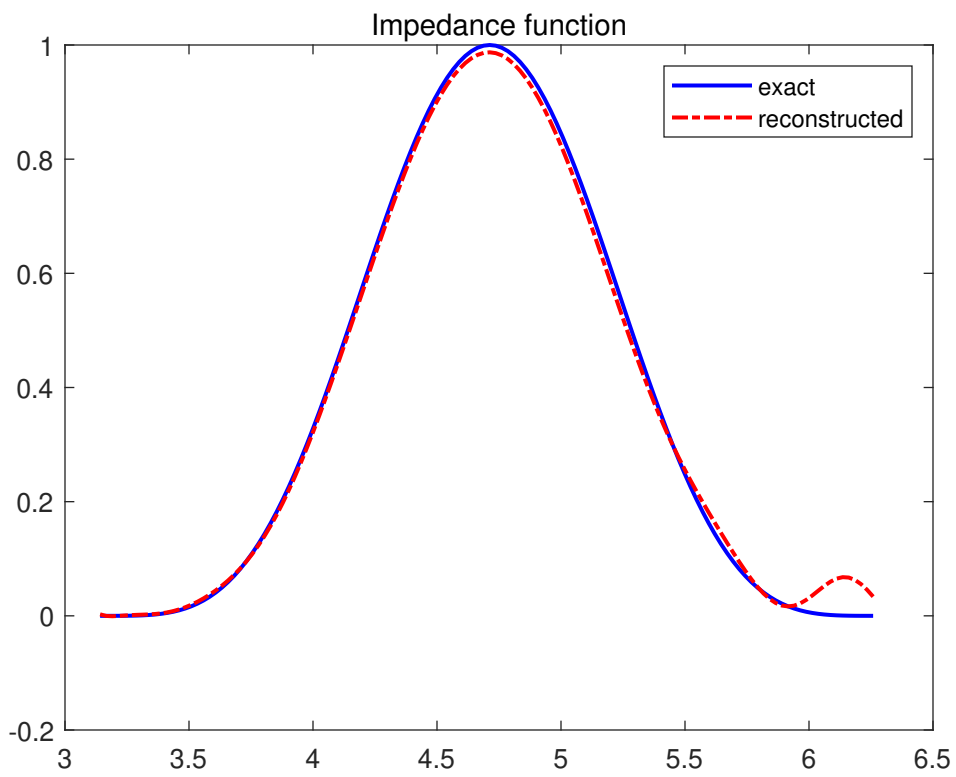


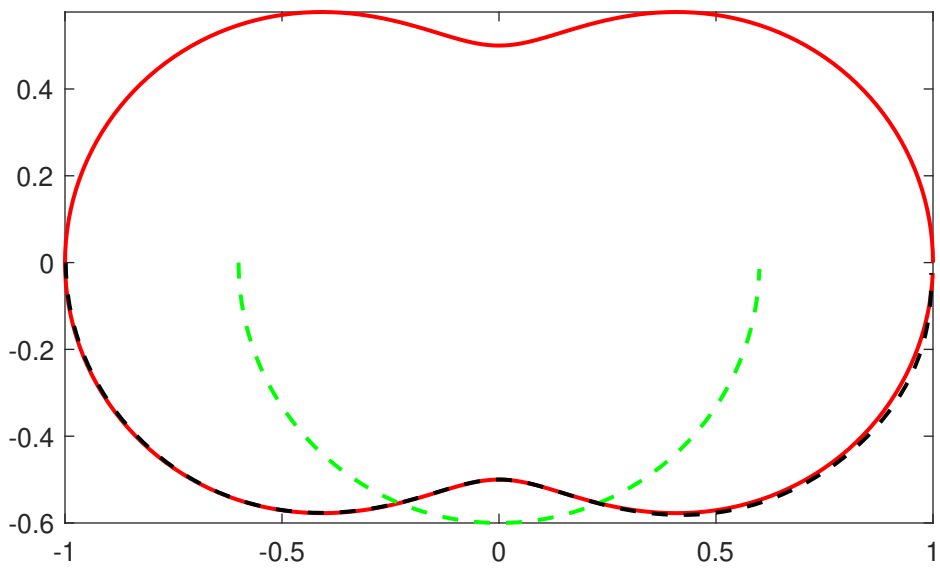


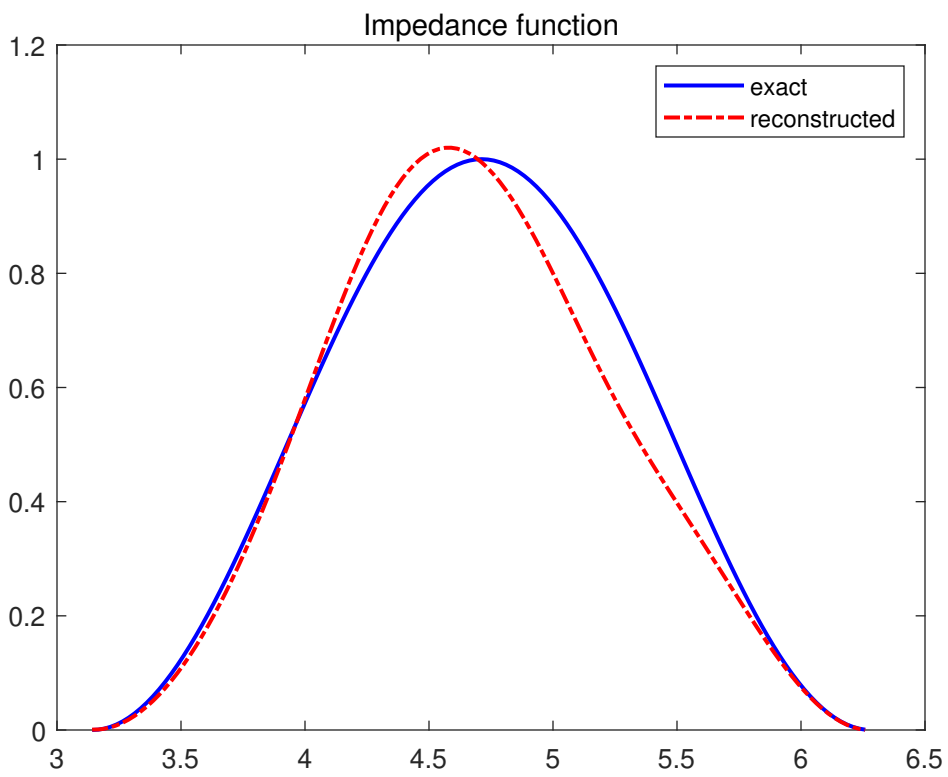


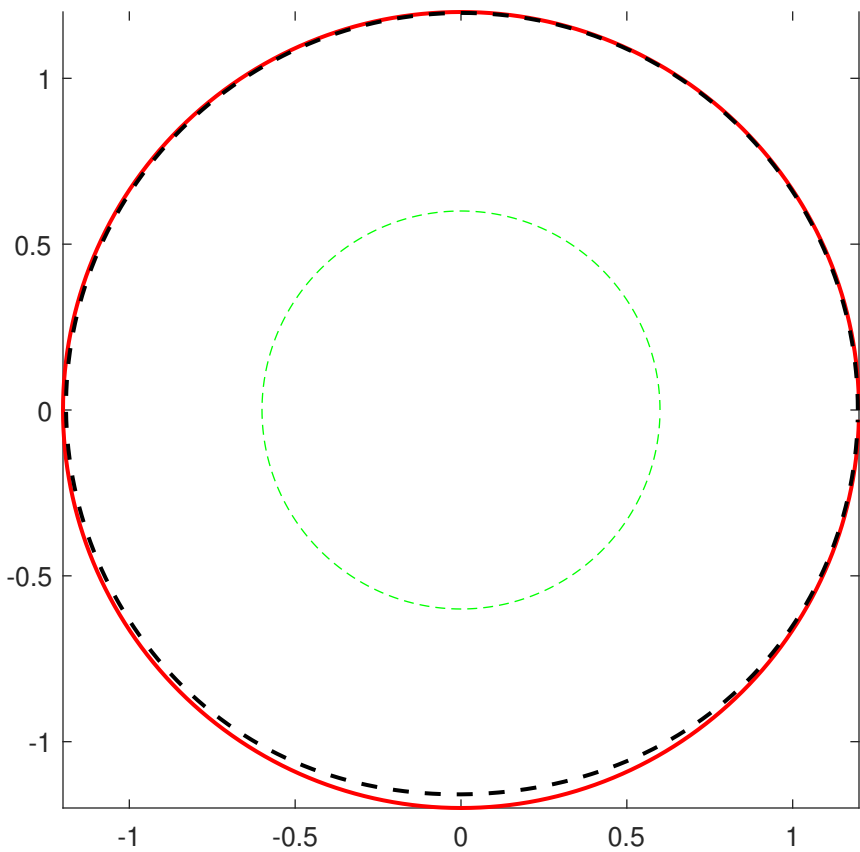


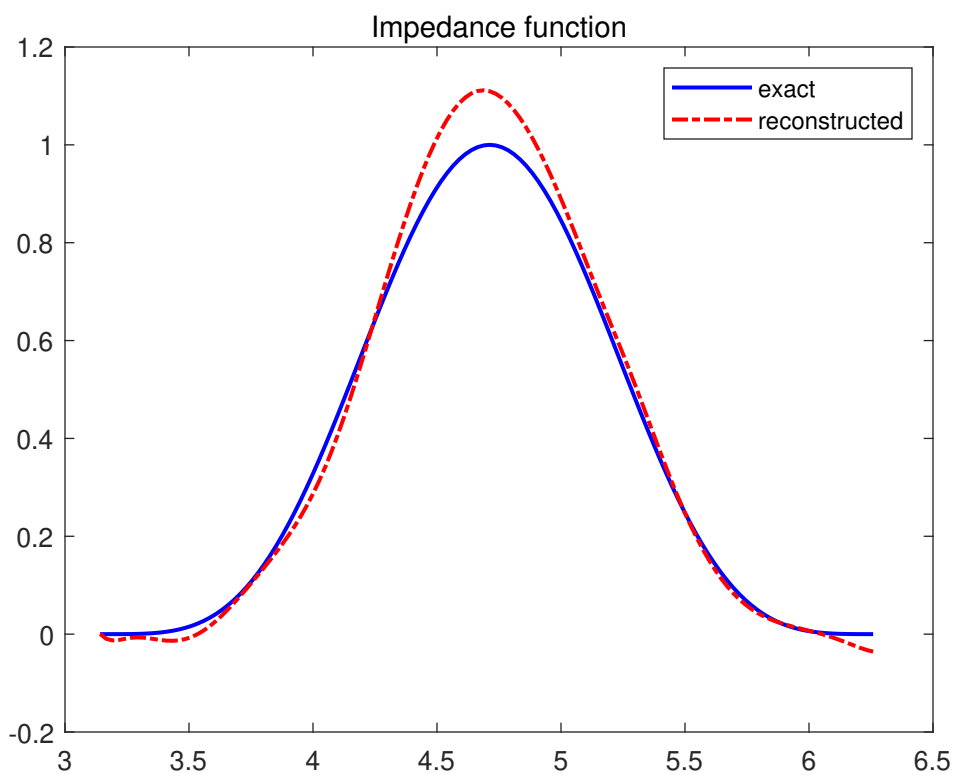


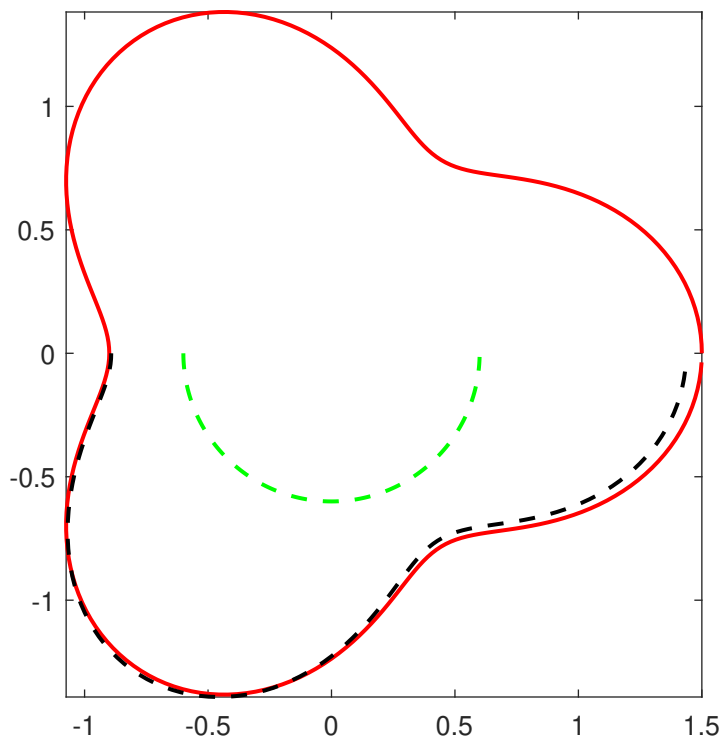




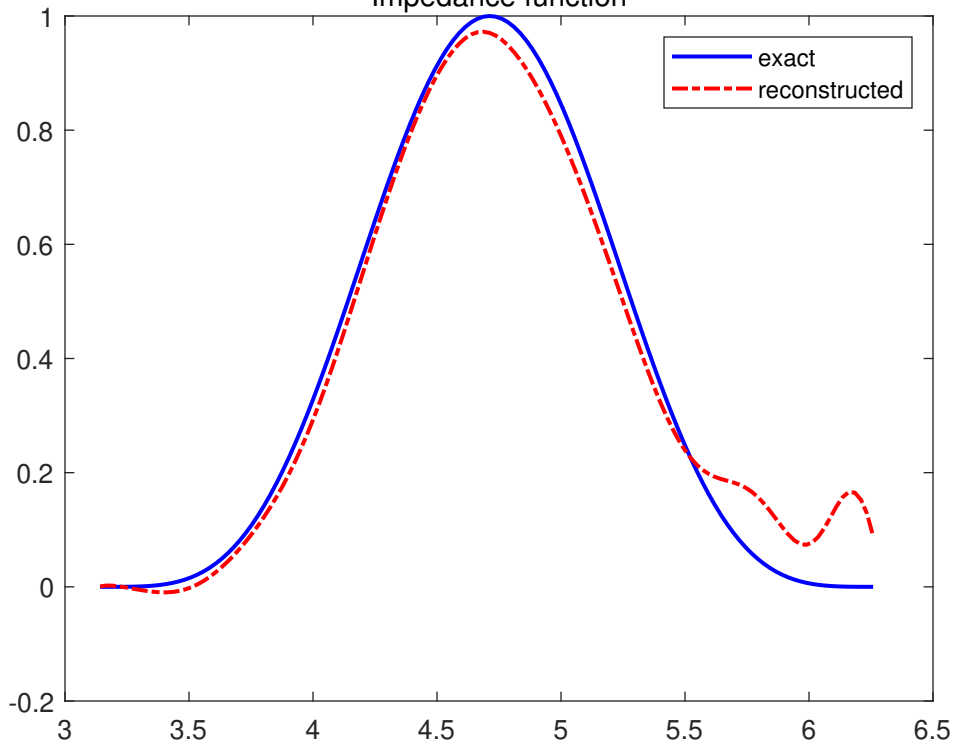


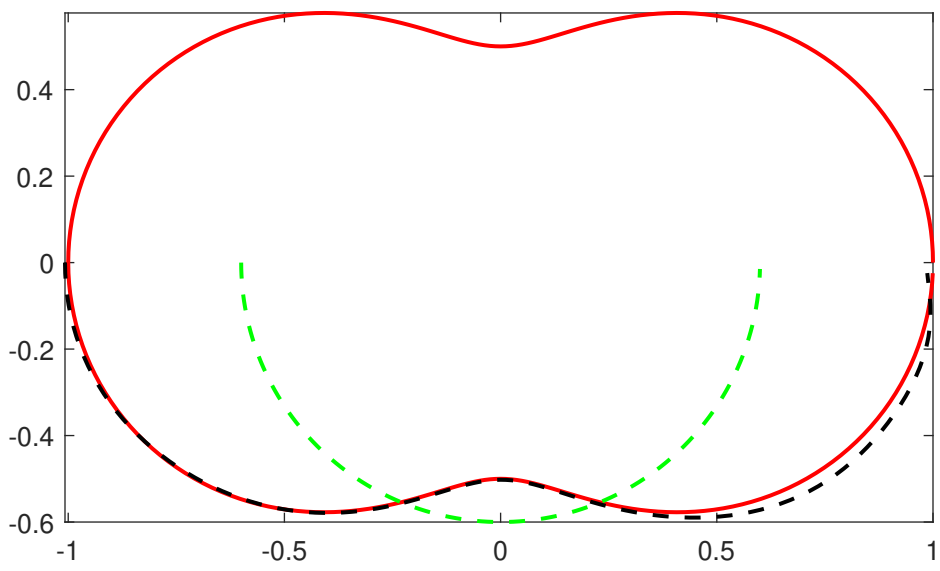


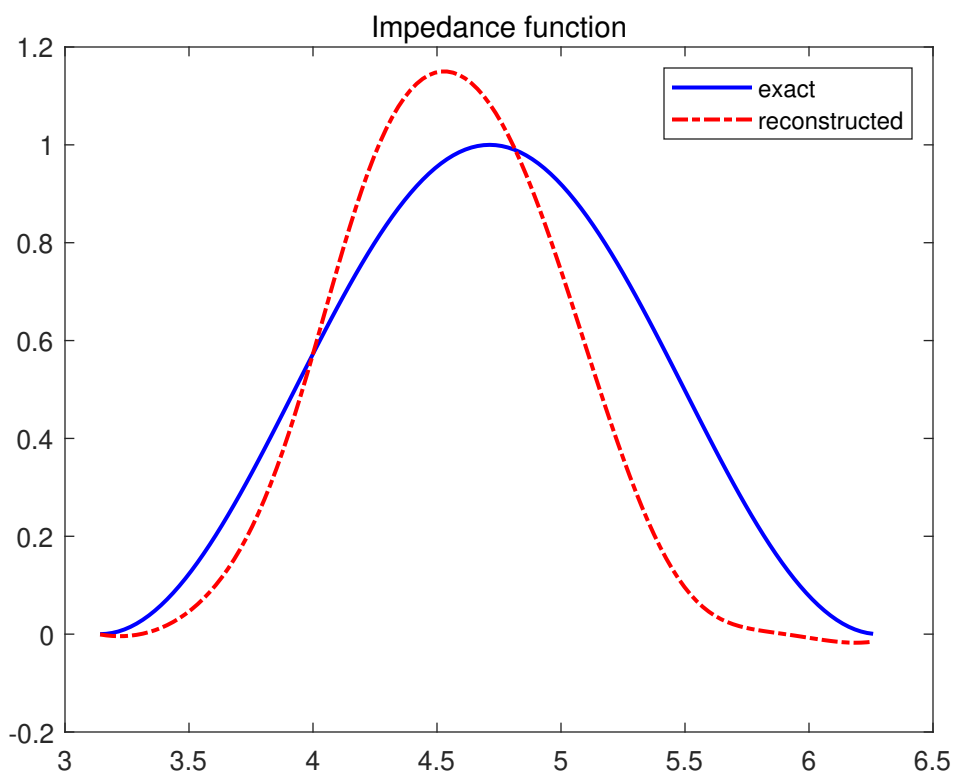


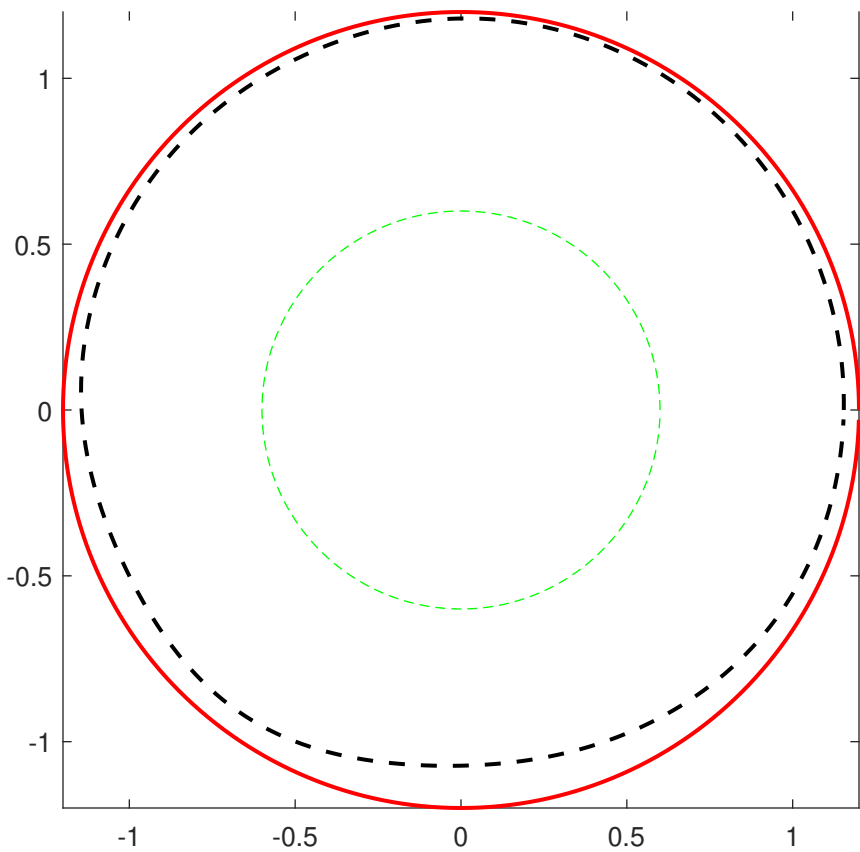


Impedance function









Impedance function

